ARTICLES

High-LET Radiolysis of Liquid Water with $^{1}H^{+}$, $^{4}He^{2+}$, $^{12}C^{6+}$, and $^{20}Ne^{9+}$ Ions: Effects of Multiple Ionization

Jintana Meesungnoen and Jean-Paul Jay-Gerin*

Département de Médecine Nucléaire et de Radiobiologie, Faculté de Médecine et des Sciences de la Santé, Université de Sherbrooke, 3001, 12e Avenue Nord, Sherbrooke (Québec) J1H 5N4, Canada

Received: February 2, 2005; In Final Form: May 11, 2005

Monte Carlo simulations are used to investigate the effects of multiple ionization of water molecules on the yields of formation of free radical and molecular species, including molecular oxygen, in the radiolysis of pure, deaerated liquid water by using different types of radiation ($^{1}H^{+}$, $^{4}He^{2+}$, $^{12}C^{6+}$, and $^{20}Ne^{9+}$ ions) up to ~900 keV/μm, at neutral pH and 25 °C. Taking into account the double, triple, and quadruple ionizations of water, the primary (or "escape") yields (at 10^{-6} s) of the various radiolytic species ($G_{e^-_{aq}}$, $G_{H^\bullet}$, G_{H_2}, $G_{^\bullet OH}$, $G_{HO_2^\bullet/O_2^{\bullet-}}$, and $G_{H_2O_2}$) are calculated as a function of the linear energy transfer (LET) of the radiation. Our results quantitatively reproduce the large increase observed in $G_{HO_2^\bullet/O_2^{\bullet-}}$ at high LET. Under the conditions of this study, the mechanisms of triple and quadruple ionizations contribute only weakly to the production of $HO_2^\bullet/O_2^{\bullet-}$. With the exception of protons, our calculations also simultaneously predict a maximum in $G_{H_2O_2}$ corresponding to the LET of ~4.5-MeV helium ions (~100 keV/μm) and ~110-MeV carbon ions (~180 keV/μm). This maximum occurs where $G_{HO_2^\bullet/O_2^{\bullet-}}$ begins to rise sharply, suggesting, in agreement with previous experimental data, that the yields of $HO_2^\bullet/O_2^{\bullet-}$ and H_2O_2 are closely linked. Moreover, our results show a steep increase in the initial and primary yields of molecular oxygen with increasing LET, giving support to the "oxygen in heavy-ion tracks" hypothesis. By contrast, it is found that, in the whole LET range considered, the incorporation of multiple ionization in the simulations has only little effect on the variation of our computed $G_{e^-_{aq}}$, $G_{H^\bullet}$, G_{H_2}, and $G_{^\bullet OH}$ values as a function of LET. As expected, $G_{e^-_{aq}}$ and $G_{^\bullet OH}$ decrease continuously with increasing LET. $G_{H^\bullet}$ at first increases and then decreases at high LET. Finally, G_{H_2} monotonically rises with increasing LET. Our calculated yield values compare generally very well with experiment.

1. Introduction

The radiolysis of pure, deaerated liquid water by low-LET (linear energy transfer, or energy loss per unit track length, -dE/dx) radiation such as ^{60}Co γ-rays, hard X-rays, fast electrons, or high-energy protons, at room temperature, is generally well understood. Briefly, it leads to the formation of the free radicals and molecular products e^-_{aq}, $H^\bullet$, $^\bullet OH$, H_2, H_2O_2, H^+, OH^-, etc.[1−3] Under ordinary irradiation conditions, these species are generated nonhomogeneously on subpicosecond time scales in small, widely separated regions of dense ionization and excitation events, commonly referred to as "spurs",[4] along the track of the ionizing radiation.[5] Owing to diffusion from their initial positions, the radiolytic products then either react within the spurs as they expand or escape into the bulk solution. The so-called "primary" radical and molecular yields (or "escape" yields) $G_{e^-_{aq}}$, $G_{H^\bullet}$, $G_{^\bullet OH}$, G_{H_2}, and $G_{H_2O_2}$ represent the numbers of species of each kind formed or destroyed per 100 eV of deposited energy that remain after spur expansion.[6] At room temperature, this spur expansion is essentially complete on the time scale of ~10^{-6} s after the initial energy deposition. At this time, the species that have escaped from spur reactions become homogeneously distributed throughout the bulk of the solution (or background) and the track of the radiation no longer exists. The radical and molecular products, considered as additions to the background, are then available for reaction with added solutes (treated as spatially homogeneous) at moderate concentrations.

With increasing LET, the nearly spherical spurs are formed increasingly closer together and eventually overlap to form dense continuous columns of species consisting initially of a cylindrical track "core" surrounded by a region of radiation effects due to the ejected secondary electrons, commonly referred to as the "penumbra".[7−11] As the interspur distance decreases, more radicals are formed in close proximity with a correspondingly increased probability of reacting with one another to produce the molecular products or to reform water. Under these conditions, the radical yields are expected to diminish as the LET is increased, whereas the molecular yields increase and the net water decomposition yield decreases.[10,12] There are two important exceptions to this rule: (i) the primary yield of hydroperoxyl/superoxide anion ($HO_2^\bullet/O_2^{\bullet-}$, p$K_a$ = 4.8) radicals increases with increasing LET, a behavior that is akin to the molecular yields,[13−22] and (ii) the primary yield of hydrogen

* Corresponding author. Tel. (1-819) 346-1110, ext. 14682/14773. Fax: (1-819) 564-5442. E-mail: jean-paul.jay-gerin@USherbrooke.ca

10.1021/jp058037z CCC: $30.25 © 2005 American Chemical Society
Published on Web 07/06/2005

peroxide (H_2O_2) rises with increasing LET to a maximum, after which it falls.[18,23]

We have recently carried out Monte Carlo track structure simulations to investigate the effects of multiple ionization of water molecules on the formation of $HO_2^{\bullet}/O_2^{\bullet-}$ and H_2O_2 in the radiolysis of liquid water with high-LET $^{12}C^{6+}$ ions up to ~430 keV/μm, at ambient temperature.[24] This innovative study was motivated by the hypothesis that multiple ionization could be responsible for the large $HO_2^{\bullet}/O_2^{\bullet-}$ yield produced in irradiated water under high-LET heavy-ion impact.[25] Indeed, incorporating the mechanisms of double and triple ionization in single ion−water collisions allowed us to quantitatively reproduce the large increase observed in $G_{HO_2^{\bullet}/O_2^{\bullet-}}$ as the LET increases above 100−200 keV/μm. The same calculations could also simultaneously predict a maximum in the variation of $G_{H_2O_2}$ with LET at ~180−200 keV/μm, in remarkable agreement with experiment. These results strongly support the importance of the role of multiple ionization in the radiolysis of water under high-LET irradiation conditions. They also suggest that multiple ionization, although infrequent relative to single ionization events, is very efficient chemically.[26]

Unfortunately, the available information on the cross-sections (probabilities) for the double (σ_{di}) and triple (σ_{ti}) ionizations of water is still quite limited.[10,27] However, using the recent *n*-fold ionization cross-section values reported by Champion[27] for the case of carbon ions in the energy range ~4.2−12 MeV/nucleon (~430−170 keV/μm) and gaseous water allowed us to obtain the good order of magnitude for both $G_{HO_2^{\bullet}/O_2^{\bullet-}}$ and $G_{H_2O_2}$, but the variation of these yields with LET was not correctly reproduced.[24] To overcome these difficulties and estimate in particular the values of the heavy ion−water cross sections in the *liquid* phase, we used[24] an original approach that consisted of treating the ratio of double-to-single ionization cross-sections ($\alpha = \sigma_{di}/\sigma_{si}$, where σ_{si} is known) in our simulations as an adjustable parameter chosen to reproduce the available experimental data of ($G_{HO_2^{\bullet}} + G_{O_2}$) as a function of LET in the $^{12}C^{6+}$ radiolysis of deaerated ferrous sulfate-cupric sulfate aqueous solutions under acidic conditions.[19,20] As for the triple ionization, σ_{ti} was assumed to be an order of magnitude less than σ_{di}.[10,27] Using the values of the double and triple ionization cross sections so obtained in our simulation code of the radiolysis of neutral water, both the magnitude of the experimental primary $HO_2^{\bullet}/O_2^{\bullet-}$ and H_2O_2 yields and their variation with LET could then be reproduced very well by our simulations.[24]

To allow a more rigorous test of our previous findings and to gain further insight into the effects of multiple ionization on the production of $HO_2^{\bullet}/O_2^{\bullet-}$ and H_2O_2 in the heavy-ion radiolysis of water at high LET, it is important to extend our previous study to other types of irradiating particles and to a wider range of LET. In the present work, we perform Monte Carlo track structure simulations that incorporate double, triple, and quadruple ionizations of water molecules to calculate the yields of formation of the various radiolytic species, including molecular oxygen, in the radiolysis of pure, deaerated liquid water by several different types of radiation ($^1H^+$, $^4He^{2+}$, $^{12}C^{6+}$, and $^{20}Ne^{9+}$ ions) at high LET up to ~900 keV/μm. This paper deals only with 25 °C results. The main features of our simulation approach are presented in the next section, followed by the results and their discussion. Conclusions are drawn in the final section.

2. Monte Carlo Simulations

The radiolysis of liquid water has been modeled by using an updated and extended version of our originally developed Monte Carlo simulation codes TRACPRO, TRACELE, and TRACIRT.[24,28−32] In this new version, which we have renamed IONLYS−IRT, significant changes in certain parameters have been made, mainly in the description of the early physical and physicochemical stages of the code. In particular, our code now employs the newly reported elastic, phonon, and vibrational electron scattering cross-sections of Michaud et al.,[33] obtained from ~1−100 eV electron-impact experiments on amorphous ice films, and increased here by a factor of about 2 to account for differences between solid- and liquid-phase cross sections.[28,34] We have also modified certain adjustable parameters that enter our code in order to reconcile the results of our simulations with (i) the recently reevaluated "initial" e_{aq}^- yield data (4.0 ± 0.2 molec./100 eV at "time zero"[35] and 4.1 ± 0.2 molec./100 eV at 20 ps,[36] as compared to the hitherto accepted value of 4.8 molec./100 eV at 100 ps[37]);[32] (ii) the newly measured e_{aq}^- decay kinetic profile in the time range from 100 ps to 10 ns;[35] and (iii) the newly determined yield of "nonscavengeable" molecular hydrogen produced on a subpicosecond time scale (0.34 molec./100 eV or ~75% of the total H_2 formed,[38] instead of the previously accepted limiting yield of 0.15 molec./100 eV[39,40]). These parameters comprise (i) the thermalization distance of subexcitation electrons (e_{sub}^-),[41] (ii) the recombination cross section of the electrons with their water parent cations prior to thermalization,[42] (iii) the branching ratios used for the different competing mechanisms in the decay of "directly" excited electronic states ($\tilde{A}^1B_1$ and $\tilde{B}^1A_1$) of water molecules and of vibrationally excited water molecules ($H_2O^*_{vib}$) formed by electron-cation geminate recombination, and (iv) the dissociative capture of electrons by water molecules.[28] The values of these parameters have been obtained here by using a global-fit procedure, which consists of *simultaneously* fitting our computed time-dependent yields of e_{aq}^- and of the other radiolytic species ($H^{\bullet}$, H_2, $^{\bullet}OH$, and H_2O_2) to experiment.[32] Using this procedure, the average electron thermalization distance calculated from our simulations is ~11.7 nm (with the corresponding average electron thermalization time of ~56 fs), a value that is somewhat larger than the typical range (or "spur" radius) of ~6.4−8.3 nm commonly used to describe the chemical evolution of the hydrated electrons in current deterministic "average" models of "spur" chemistry for low-LET radiation.[10,43−45] As for the geminate electron−cation recombination probability, 25.5% of the subexcitation electrons are found to initially recombine with their water parent cations (on the average, this recombination occurs in the first steps of the e_{sub}^- random walk, that is, in times as short as a few femtoseconds)[42] to form $H_2O^*_{vib}$. This latter value is consistent with the prompt electron−cation recombination (≥15%) in water radiolysis reported recently by Bartels et al.[46] The revised values of the branching ratios used for the different dissociative decay channels of $H_2O^*_{vib}$ are shown in Table 1A. We should note here that the various decay channels of directly excited electronic states of water molecules have little effect in the yield calculations. Nevertheless, those branching ratios have been slightly modified with respect to those previously published[28] (see Table 1B). Finally, the maximum value of the dissociative electron attachment cross section has been adjusted to ~4.5×10^{-18} cm^2 at ~8.6 eV in order to reproduce the prompt "nonscavengeable" yield of H_2 observed experimentally.[28,47] This value compares well with that determined recently in amorphous ice (2.7×10^{-18} cm^2)[33] and with the corresponding gas-phase value (6.7×10^{-18} cm^2).[48]

During the physical stage, the energy deposition by the incident charged particle and by all the secondary electrons that

TABLE 1: Revised Branching Ratios Used in Our Simulations for the Different Competing Mechanisms in the Fate of (A) Vibrationally Excited Water Molecules ($H_2O^*_{vib}$) Formed by Recombination of a Subexcitation Electron (e^-_{sub}) with its Water Parent Cation ($H_2O^{\bullet+}$)[a] and (B) Directly Excited Electronic States ($\tilde{A}^1B_1$ and $\tilde{B}^1A_1$) of Water Molecules[b]

(A)					
$H_2O^{\bullet+} + e^-$	→	$H_2O^*_{vib}$			
$H_2O^*_{vib}$	→	nondissociative deexcitation	45% (35%)	→	H_2O + release of thermal energy
	→	dissociative deexcitation	55% (65%)	→	$H^\bullet + {}^\bullet OH$ 79% (79.8%) $2H^\bullet + O(^3P)$ 8% (5.5%) $H_2 + O(^1D)$ 13% (14.7%)
(B)					
$H_2O^*(\tilde{A}^1B_1)$	→	nondissociative deexcitation	45% (35%)	→	H_2O
	→	dissociative deexcitation	55% (65%)	→	$H^\bullet + {}^\bullet OH$
$H_2O^*(\tilde{B}^1A_1)$	→	autoionization	50% (50%)	→	$H_2O^{\bullet+} + e^-$
	→	nondissociative deexcitation	22.5% (17.5%)	→	H_2O
	→	dissociative deexcitation	27.5% (32.5%)	→	$H^\bullet + {}^\bullet OH$ 79% (78%) $2H^\bullet + O(^3P)$ 8% (12%) $H_2 + O(^1D)$ 13% (10%)

[a] Previously employed values from ref 32 are given in parentheses. [b] Previously employed values from ref 28 are given in parentheses.

it has generated occurs through the slowing down of those particles via a variety of elastic and inelastic scattering processes, including ionization, electronic and vibrational excitation of single water molecules, and excitation of plasmon-type collective modes. The details of our track structure simulation modeling and the scattering cross-sections used are described in our earlier publications.[24,28−32] To take into account the effects of multiple ionization under high-LET heavy-ion impact, the model has been extended to incorporate double, triple, and quadruple ionization processes in single ion−water collisions.[24,25] Ionizations of higher multiplicity are neglected as their occurrence is much less probable in the range of LET of interest here. In the simulations, a value of 40 eV is accepted for the total energy needed to eject two electrons from a water molecule (double-ionization energy) as taken from gas-phase studies,[49] whereas the values for the triple- and quadruple-ionization energies (chosen equal to 65 and 88 eV, respectively) are assumed to be near the energies needed for the triple and quadruple ionizations of oxygen.[50] Unfortunately, little is known yet about the values of the cross sections for the double (σ_{di}), triple (σ_{ti}), and quadruple (σ_{qi}) ionizations of water.[10,27] In this study, σ_{di} is deduced from the knowledge of the ratio $\alpha = \sigma_{di}/\sigma_{si}$ and Rudd's semiempirical single ionization cross sections (σ_{si}) for proton impact on water vapor[51] (adapted here to the liquid phase as previously described[28] and extended to collisions by any other ion projectile of the same velocity according to a Z^2 scaling law, where Z is the charge state of the ion[52]). Following the approach used previously,[24] we have treated α in our simulations as an adjustable parameter chosen to get the best fit of the experimental values of ($G_{HO_2^\bullet} + G_{O_2}$) as a function of LET in the radiolysis of air-free aqueous $FeSO_4$ (1 mM)−$CuSO_4$ (10 mM) solutions with $^1H^+$, $^4He^{2+}$, $^{12}C^{6+}$, and $^{20}Ne^{9+}$ ions under acidic (0.005 M H_2SO_4) conditions.[19,20,53,54] As shown in our previous paper,[24] this approach offers an original tool to estimate the ratio σ_{di}/σ_{si} for heavy ion−water collisions in the *liquid* phase. As for the triple and quadruple ionizations, we assume that, for the range of impacting ion energies considered in this work, $\sigma_{ti} = \alpha^2\,\sigma_{si}$ and $\sigma_{qi} = \alpha^3\,\sigma_{si}$, where $\alpha < 0.5$.[27] We have also multiplied the total cross-sections for all interaction processes induced by ions by an energy-dependent factor that constrains the LET of the irradiating ions to conform with the recommended values of Watt.[55] Finally, at the incident ion energies of interest here, interactions involving electron capture and loss by the moving ion (charge-changing collisions) have been neglected.[56]

The energy that has been so deposited in the medium is then used to produce the "initial" radical and molecular species of the radiolysis, distributed in a specific, highly nonhomogeneous track structure which depends on the primary ion type and energy. The physicochemical stage consists of the processes that lead to the establishment of thermal equilibrium in the system. Its duration is of the order of 10^{-12} s for aqueous solutions. Among those processes, the production of $HO_2^\bullet/O_2^{\bullet-}$ via the double ionization of water is assumed to involve oxygen atoms[19,57−59] formed in their ^3P ground state,[25] according to

$$H_2O^{2+} + 2\,H_2O \rightarrow 2\,H_3O^+ + O(^3P) \qquad \text{(R1)}$$

at very short times, followed by

$${}^\bullet OH + O(^3P) \rightarrow HO_2^\bullet \qquad \text{(R2)}$$

It should be recalled here that the O atoms produced in their singlet ^1D state react rapidly with water.[60,61] In contrast, the ground-state $O(^3P)$ atoms are rather inert to water[60,62] and will then react efficiently with $^\bullet OH$ radicals in the heavy particle track core because of the very high local concentration of radicals.[25] For the triple and quadruple ionizations of water molecules, we assume that they directly lead to the formation of $HO_2^\bullet/O_2^{\bullet-}$ and molecular oxygen by acid−base re-equilibrations, respectively, according to the following overall reactions:[25]

$$H_2O^{\bullet 3+} + 4H_2O \rightarrow 3H_3O^+ + HO_2^\bullet \qquad \text{(R3)}$$

and

$$H_2O^{4+} + 5H_2O \rightarrow 4H_3O^+ + O_2 \qquad \text{(R4)}$$

The H_3O^+ ions formed in reactions R1, R3, and R4 are positioned at 0.3 nm from their respective coproducts $O(^3P)$, $HO_2^\bullet$, and O_2, which are held in place. This is the same separation as that used between H_3O^+ and the $^\bullet OH$ radical in our simulation of events following the dissociation of $H_2O^{\bullet+}$.[28] In addition, the emission angles for the secondary electrons ejected from the target by the impacting ion are separated by 180°, 120°, and 90° when dealing with double, triple, and

quadruple ionization, respectively, and the total incident energy deposited at each point of interaction (after subtraction of the required ionization energy of the water molecule) is equally distributed between the ejected electrons.

All of the events of the physical and physicochemical stages are handled by our revised step-by-step simulation program IONLYS (which replaces TRACPRO and TRACELE)[24,28−32] extended here to incorporate multiple ionization of water molecules as described above. The complex spatial distribution of reactants at $\sim 10^{-13}$ s, which is provided as an output of this program, is then used directly as the starting point for the subsequent nonhomogeneous chemical stage. This third and final stage, during which the various radiolytic species diffuse and react with one another (or with the environment) until all spur or track reactions are complete ($\sim 10^{-6}$ s), is covered by our IRT program.[24,28−32] This program employs the independent reaction times (IRT) method[63] to model the chemical development that occurs during this stage and to simulate the formation of measurable product yields. Its implementation has been described in detail,[29] and its validity has been established through a comparison with a full step-by-step Monte Carlo simulation.[64]

The reaction scheme and reaction parameters, as well as the diffusion coefficients of reactive species used in our IRT program for pure liquid water, are given in Tables 1 and 2 of ref 29. Only slight adjustments were made in some reaction rate constants and diffusion coefficients to take account of the latest data available from the literature. To simulate the radiolysis of the Fe^{2+}/Cu^{2+} system in deaerated 0.005 M H_2SO_4 aqueous solutions (pH $\approx$ 2.1), we have supplemented the pure-water reaction scheme to include the 31 reactions listed in Table 2. In addition, we have introduced the effects due to the ionic strength of the solutions[78] for the two reactions[31]

$$H^+ + e_{aq}^- \rightarrow H^\bullet$$

and

$$H^+ + OH^- \rightarrow H_2O$$

as well as for all reactions between ions given in Table 2. The rate constants for those various reactions, corrected for these ionic-strength effects, have been used in the present study.[79]

Finally, the influence of the LET on the yields of the various radiation-induced species in neutral water at ambient temperature has been investigated by varying the incident ion energy from $\sim$300 to 0.15 MeV ($\sim$0.3−70 keV/μm) for $^1H^+$, $\sim$300 to 0.3 MeV/nucleon ($\sim$1.25−213 keV/μm) for $^4He^{2+}$, $\sim$300 to 1.25 MeV/nucleon ($\sim$12−604 keV/μm) for $^{12}C^{6+}$, and $\sim$300 to 3.2 MeV/nucleon ($\sim$25−938 keV/μm) for $^{20}Ne^{9+}$. The calculations are performed by simulating short ($\sim$1.5−100 μm) ion track segments, over which the energy and LET of the ion are well defined and remain nearly constant. Typically, $\sim$5000 to 400 000 reactive chemical species are generated in those simulated track segments (depending on the irradiating-ion type and energy), thus ensuring only small statistical fluctuations in the determination of average yields.

TABLE 2: Reaction Scheme Considered in Our Simulations to Model the Radiolysis of Deaerated 0.005 M H_2SO_4 Solutions of $FeSO_4-CuSO_4$ (pH $\sim$ 2.1) at 25 °C

reaction	k (M^{-1} s^{-1})
$H^\bullet + Fe^{2+} \rightarrow Fe^{3+} + H^-$	1.3×10^{7} [a,b]
$H^\bullet + Cu^{2+} \rightarrow Cu^{+} + H^+$	9.1×10^{7} [c]
$H^\bullet + Fe^{3+} \rightarrow Fe^{2+} + H^+$	1.0×10^{8} [a,b]
$H^\bullet + Cu^{+} \rightarrow CuH^+$	5.0×10^{9} [c]
$H^\bullet + SO_4^{\bullet-} \rightarrow HSO_4^-$	1.0×10^{10} [d]
$H^\bullet + S_2O_8^{2-} \rightarrow SO_4^{\bullet-} + HSO_4^-$	2.5×10^{7} [c]
$^\bullet OH + Fe^{2+} \rightarrow Fe^{3+} + OH^-$	3.4×10^{8} [a,b]
$^\bullet OH + Cu^{2+} \rightarrow Cu^{3+} + OH^-$	3.5×10^{8} [c]
$^\bullet OH + Cu^{+} \rightarrow Cu^{2+} + OH^-$	2.0×10^{10} [e]
$^\bullet OH + HSO_4^- \rightarrow H_2O + SO_4^{\bullet-}$	1.5×10^{5} [f,g]
$e_{aq}^- + Fe^{2+} \rightarrow Fe^{+}$	1.2×10^{8} [b]
$e_{aq}^- + Cu^{2+} \rightarrow Cu^{+}$	3.8×10^{10} [h]
$e_{aq}^- + Fe^{3+} \rightarrow Fe^{2+}$	2.0×10^{10} [a,b]
$e_{aq}^- + Cu^{+} \rightarrow Cu$	2.7×10^{10} [c]
$e_{aq}^- + S_2O_8^{2-} \rightarrow SO_4^{\bullet-} + SO_4^{2-}$	1.2×10^{10} [c]
$H_2O_2 + SO_4^{\bullet-} \rightarrow HO_2^\bullet + HSO_4^-$	1.2×10^{7} [i]
$HO_2^\bullet + Fe^{2+} \rightarrow Fe^{3+} + HO_2^-$	7.9×10^{5} [a]
$HO_2^\bullet + Cu^{2+} \rightarrow Cu^{+} + O_2 + H^+$	1.2×10^{8} [a,j,k]
$HO_2^\bullet + Fe^{3+} \rightarrow Fe^{2+} + O_2 + H^+$	2.0×10^{4} [k]
$HO_2^\bullet + Cu^{+} \rightarrow Cu^{2+} + HO_2^-$	2.3×10^{9} [k]
$O_2^{\bullet-} + Cu^{2+} \rightarrow Cu^{+} + O_2$	1.1×10^{10} [j,k]
$O^{\bullet-} + Fe^{2+} \rightarrow Fe^{3+} + OH^-$	3.8×10^{9} [c]
$O_2 + Cu^{+} \rightarrow Cu^{2+} + O_2^{\bullet-}$	4.6×10^{5} [l]
$CuH^+ + H^+ \rightarrow Cu^{2+} + H_2$	1.0×10^{6} [m]
$OH^- + SO_4^{\bullet-} \rightarrow {}^\bullet OH + SO_4^{2-}$	8.3×10^{7} [i]
$Fe^{2+} + SO_4^{\bullet-} \rightarrow Fe^{3+} + SO_4^{2-}$	9.9×10^{8} [i]
$Cu^{+} + SO_4^{\bullet-} \rightarrow Cu^{2+} + SO_4^{2-}$	1.8×10^{10} [n]
$Cu^{+} + Fe^{3+} \rightarrow Cu^{2+} + Fe^{2+}$	5.5×10^{6} [l]
$Cu^{3+} + Fe^{2+} \rightarrow Cu^{2+} + Fe^{3+}$	3.3×10^{8} [l]
$CuH^+ + Cu^{2+} \rightarrow 2\,Cu^{+} + H^+$	7.0×10^{6} [m]
$SO_4^{\bullet-} + SO_4^{\bullet-} \rightarrow S_2O_8^{2-}$	4.4×10^{8} [i]

[a] Reference 65. [b] Reference 66. [c] Reference 67. [d] Reference 68. [e] Reference 69. [f] Reference 31. [g] Reference 70. [h] Reference 71. [i] Reference 72. [j] Reference 73. [k] Reference 74. [l] Reference 75. [m] Reference 76. [n] Reference 77.

3. Results and Discussion

As described above, the ratio of double-to-single ionization cross sections $\alpha = \sigma_{di}/\sigma_{si}$ is treated as an adjustable parameter and obtained from our simulations by fitting the available data[19,20] of ($G_{HO_2^\bullet} + G_{O_2}$) in the $^1H^+$, $^4He^{2+}$, $^{12}C^{6+}$, and $^{20}Ne^{9+}$ radiolysis of deaerated aqueous $FeSO_4-CuSO_4$ solutions under acidic conditions over the range of ion energies studied experimentally. The values of α so obtained are shown in Figure 1 for the four ion types used as a function of the ion energy per nucleon divided by the projectile charge state (E_{ion}/Z). The corresponding σ_{di}/σ_{si} values reported by Champion[27] for various ions and *gaseous* targets, extrapolated to the case of any heavy ion and to water molecules, are also included in Figure 1 for the sake of comparison. It is seen that, in contrast to Champion's values,[27] our values of α do not follow a unique law, independent of the projectile ion. In fact, the present data show that the ratio σ_{di}/σ_{si} depends on the type of the impacting ion and, for a given value of E_{ion}/Z, increases from protons ($Z = 1$) to neon ions ($Z = 9$). Moreover, even if our σ_{di}/σ_{si} values bear some qualitative resemblance in trends with those of Champion,[27] they generally differ appreciably in absolute value from the latter, except for $^{12}C^{6+}$ ions around 2.5−5 MeV/nucleon ($\sim$440−280 keV/μm) where the two sets of values are quite comparable. The source of these differences in the σ_{di}/σ_{si} values is not obvious, although they are undoubtedly a manifestation of a subtle interplay during the collision between the ion-target interaction and the effects of electron−electron correlations.[51,80] This is an area where very little is known and where more experimental and theoretical work is required. In this respect, the σ_{di}/σ_{si} values reported here could provide a useful test for theories calculating many-electron emission cross sections in single ionizing collisions.

Using these values of σ_{di}/σ_{si} in our simulation code of the radiolysis of pure, deaerated, *neutral* water with $^1H^+$, $^4He^{2+}$, $^{12}C^{6+}$, and $^{20}Ne^{9+}$ ions, we have then calculated $G_{HO_2^\bullet/O_2^{\bullet-}}$ and

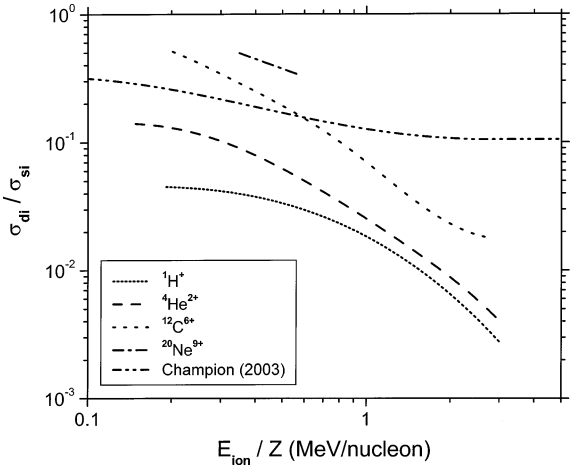

Figure 1. Ratio of the double to single ionization cross-sections ($\alpha = \sigma_{di}/\sigma_{si}$) as a function of E_{ion}/Z, where E_{ion} is the ion energy per nucleon and Z is the projectile charge state. The short-dot, dash, dot, and dash-dot lines represent the values of α obtained from our Monte Carlo simulations of the radiolysis of air-free aqueous $FeSO_4$ (1 mM)−$CuSO_4$ (10 mM) solutions under acidic (0.005 M H_2SO_4) conditions for $^1H^+$, $^4He^{2+}$, $^{12}C^{6+}$, and $^{20}Ne^{9+}$ ions, respectively. In those simulations, performed at 25 °C, α is treated as an adjustable parameter chosen to get the best fit of the experimental data of LaVerne and Schuler (ref 20) of ($G_{HO_2^\bullet} + G_{O_2}$) as a function of LET (see text). The values of α reported by Champion for a variety of ions at intermediate velocities and gaseous water (solid line in Figure 1 in ref 27) are also shown for the sake of comparison (dash-dot-dot line).

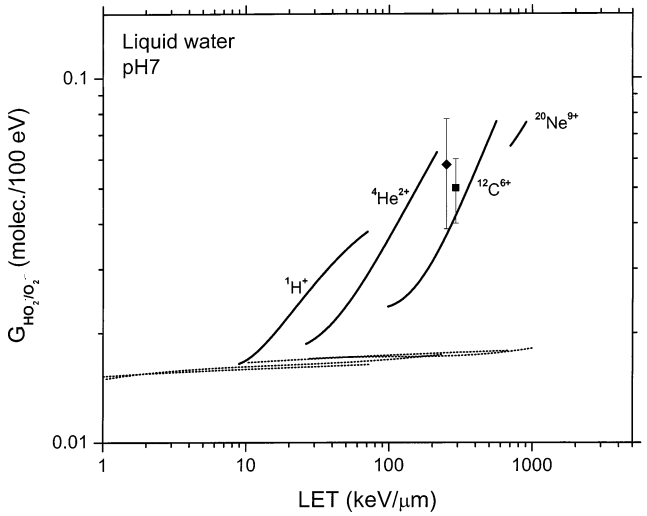

Figure 2. Variation of the primary $HO_2^\bullet/O_2^{\bullet-}$ yield ($G_{HO_2^\bullet/O_2^{\bullet-}}$) (in molec./100 eV) of the radiolysis of deaerated liquid water by $^1H^+$, $^4He^{2+}$, $^{12}C^{6+}$, and $^{20}Ne^{9+}$ ions as a function of LET up to ∼900 keV/μm, at neutral pH and 25°C. The solid lines represent the results of our Monte Carlo simulations incorporating the double, triple, and quadruple ionizations of water molecules, obtained at 10^{-6} s (see text). The short-dot lines correspond to our $G_{HO_2^\bullet/O_2^{\bullet-}}$ values calculated as a function of LET without including the mechanism of multiple ionization of water. Experimental yields (pH ≈ 7): (◆) $^{36}S^{16+}$ ions (77 MeV/nucleon, LET ∼ 250 keV/μm) (ref 21), and (■) $^{40}Ar^{18+}$ ions (70 MeV/nucleon, LET ∼ 290 keV/μm) (ref 81).

$G_{H_2O_2}$ (at 10^{-6} s) as a function of LET up to ∼900 keV/μm, at 25 °C. The results are shown in Figures 2 and 3, respectively, along with experimentally determined yields from the literature.[15,21,23,81−84] As can be seen in Figure 2, our curves of $G_{HO_2^\bullet/O_2^{\bullet-}}$ versus LET calculated without including the mechanism of multiple ionization of water cannot account quantitatively for the totality of the measured $HO_2^\bullet/O_2^{\bullet-}$ yield[21,81] at

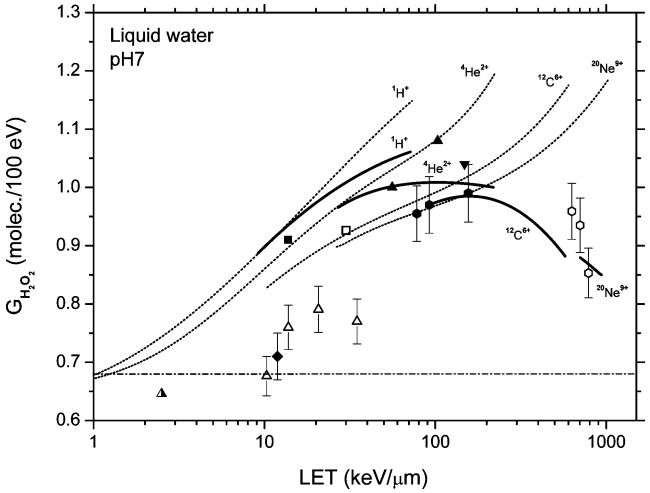

Figure 3. Variation of the primary H_2O_2 yield ($G_{H_2O_2}$) (in molec./100 eV) of the radiolysis of deaerated liquid water by $^1H^+$, $^4He^{2+}$, $^{12}C^{6+}$, and $^{20}Ne^{9+}$ ions as a function of LET up to ∼900 keV/μm, at neutral pH and 25°C. The solid lines represent the results of our Monte Carlo simulations incorporating the double, triple, and quadruple ionizations of water molecules, obtained at 10^{-6} s (see text). The short-dot lines correspond to our $G_{H_2O_2}$ values calculated as a function of LET without including the mechanism of multiple ionization of water. Experimental yields (pH ≈ 7): $^1H^+$ [(△), ref 23; (▲), ref 82], $^2H^+$, at one-half energy [(■), ref 15; (◆), ref 83], $^4He^{2+}$ [(▲), ref 15; (⬢), ref 23; (▼), ref 84], and $^{12}C^{6+}$ [(○), ref 23; (□), ref 82]. The dash−dot line represents the limiting primary H_2O_2 yield obtained with ^{60}Co γ-rays or fast electrons (∼0.68 molec./100 eV) (ref 2).

high LET. However, when the double, triple, and quadruple ionizations are incorporated in the simulations for the four irradiating ions studied, the magnitude of the $HO_2^\bullet/O_2^{\bullet-}$ escape yields so obtained compares well with experiment. Figure 2 also shows that, for different incident ions of equal LET but different velocities, $G_{HO_2^\bullet/O_2^{\bullet-}}$ decreases as the ion velocity increases.[85] This irradiating-ion dependence of the yields at a given LET indicates, as it has been frequently noted,[2,10−12,56,86−90] that LET is not a unique parameter to correctly describe the radiation chemical effects within heavy ion tracks. This is explained by the greater mean energy of ejected electrons (the so-called low-LET "short" and "branch" tracks in the terminology of Mozumder and Magee,[9,91] or "δ-rays") from the higher velocity ion, which will travel to a greater average distance away from the track core and so lead to a greater dispersion of the initial radical positions around the track. In other words, the actual mean initial volume density of free radicals formed in the track will be lower. Under these conditions, a greater fraction of those radicals will be allowed to escape recombination as they subsequently diffuse with consequent tendency for increase in the radical yields measured after track expansion, along with decreased molecular product yields. However, the decrease observed in our simulated $G_{HO_2^\bullet/O_2^{\bullet-}}$ values with increasing ion velocity at the same LET (the production of $HO_2^\bullet/O_2^{\bullet-}$ is lower for the heavier ions) supports our assumption made in reaction R2 that $HO_2^\bullet$ is formed by radical combination processes within the track,[92] in quite the same fashion as the general formation of molecular species.[10,11] LaVerne and co-workers[19] also concluded that the yield of ($HO_2^\bullet + O_2$) is significant only at high LET and that it is produced mainly in the heavy-particle track core at high radical concentration. It is finally worth noting that independent simulations incorporating the sole mechanism of double ionization of water molecules have shown that triply and quadruply charged water ions make in fact only a minor contribution to $G_{HO_2^\bullet/O_2^{\bullet-}}$ and $G_{H_2O_2}$ (∼15% and 2% for

~555 keV/μm $^{12}C^{6+}$ ions, respectively) under the conditions $\sigma_{ti} = \alpha^2\ \sigma_{si}$ and $\sigma_{qi} = \alpha^3\ \sigma_{si}$ ($\alpha < 0.5$) adopted in this study (data not shown).

Quite similarly, Figure 3 shows that our values of $G_{H_2O_2}$ calculated without multiple ionization of water continuously increase with increasing LET. However, when the double, triple, and quadruple ionizations are incorporated in the simulations, the curves of $G_{H_2O_2}$ versus LET first rise, then bend downward ($^1H^+$) and, at higher LET, reach a maximum ($^4He^{2+}$ and $^{12}C^{6+}$), after which they fall. This maximum is relatively shallow for $^4He^{2+}$ ions but more pronounced for $^{12}C^{6+}$ ions. Its position also slightly shifts to higher LET as the ion charge increases, going from ~100 keV/μm for ~4.5 MeV $^4He^{2+}$ ions to ~180 keV/μm for ~110 MeV $^{12}C^{6+}$ ions. For $^{20}Ne^{9+}$ ions, it is apparent from Figure 3 that a maximum should also exist, perhaps near ~200 keV/μm, even if we could not have a better definition of our curve of $G_{H_2O_2}$ below ~700 keV/μm due to a lack of experimental data of ($G_{HO_2^\bullet} + G_{O_2}$) in the radiolysis of the Fe^{2+}/Cu^{2+} system with high-energy $^{20}Ne^{9+}$ ions under acidic conditions.[19,20] These results are in good agreement with experiment, especially with the recent measurements of Pastina and LaVerne[23] for $^4He^{2+}$ and $^{12}C^{6+}$ ions and of Wasselin-Trupin et al.[82] for $^{12}C^{6+}$ ions. Moreover, if we consider the curve of $G_{H_2O_2}$ as a function of LET that includes the ensemble of our four calculated $G_{H_2O_2}$(LET) curves for the different ions studied, we can estimate an overall maximum around 100−200 keV/μm, which is in remarkable agreement with the early observations of Bibler[16] and of Burns and Sims.[18] As observed with $HO_2^\bullet/O_2^{\bullet-}$, the H_2O_2 yields are also both LET and irradiating-ion dependent. For different impacting ions of equal LET but different velocities, Figure 3 shows that $G_{H_2O_2}$ decreases as the ion velocity increases,[85] from protons to neon ions. As discussed above, this result conforms well to the general model of formation of molecular species. Finally, Figures 2 and 3 also indicate that, for each ion investigated, the maximum in the value of $G_{H_2O_2}$ occurs precisely where $G_{HO_2^\bullet/O_2^{\bullet-}}$ begins to rise sharply. This is in excellent accord with experiment and clearly shows that the yields of $HO_2^\bullet/O_2^{\bullet-}$ and H_2O_2 are closely linked.[18,24] In fact, hydrogen peroxide is formed within the tracks mainly by the combination reaction of two $^\bullet$OH radicals produced in the decomposition of water:

$$^\bullet OH + {}^\bullet OH \rightarrow H_2O_2 \qquad (R5)$$

As $^\bullet$OH reacts with O(^{3}P) by reaction R2, this reaction competes with reaction R5, causing a decrease in the observed H_2O_2 yield at high LET. This very good agreement between theory and experiment supports a posteriori our assumption[25] made in reaction R1 that, for the high-LET range considered here, O atoms are primarily produced in their ^{3}P ground state (rather than in their singlet ^{1}D state).

To gain further insight into the effects of multiple ionization of water on $G_{HO_2^\bullet/O_2^{\bullet-}}$ and $G_{H_2O_2}$ in the high-LET heavy-ion water radiolysis, it is of interest to examine the unfolding of the various reactions that contribute to the formation or decay of $HO_2^\bullet/O_2^{\bullet-}$ and H_2O_2 in the ion tracks as they expand by diffusion. This can readily be done with our Monte Carlo simulations, which enable us to determine quantitatively the time dependence of each reaction. The main reactions that are involved in the primary yields of $HO_2^\bullet/O_2^{\bullet-}$ and H_2O_2 in the case of pure, deaerated liquid water irradiated by 24 MeV $^{12}C^{6+}$ ions (~500 keV/μm) at 25 °C are listed in Tables 3 and 4, respectively. The importance of these reactions can be quantified by the yield variations $\Delta G(HO_2^\bullet/O_2^{\bullet-})$ and $\Delta G(H_2O_2)$ that they cause over the time interval of nonhomogeneous track chemistry

TABLE 3: Main Track Reactions that Contribute to the Formation and Decay of $HO_2^\bullet/O_2^{\bullet-}$ in Our Monte Carlo Simulations of the Radiolysis of Pure, Deaerated Liquid Water by 24 MeV $^{12}C^{6+}$ Ions (~500 KeV/μM) at 25 °C and in the Time Interval ~10^{-12}−10^{-6} s

reaction[a]	symbol[b]
$^\bullet OH + O(^3P) \rightarrow HO_2^\bullet$	(R2)
$^\bullet OH + HO_2^\bullet \rightarrow O_2 + H_2O$	(R6)
$^\bullet OH + O_2^{\bullet-} \rightarrow O_2 + OH^-$	(R7)
$e_{aq}^- + HO_2^\bullet \rightarrow HO_2^-$	(R8)
$e_{aq}^- + O_2^{\bullet-} \rightarrow H_2O_2 + 2\ OH^-$	(R9)
$e_{aq}^- + O_2 \rightarrow O_2^{\bullet-}$	(R10)
$H^\bullet + O_2 \rightarrow HO_2^\bullet$	(R11)
$H^\bullet + HO_2^\bullet \rightarrow H_2O_2$	(R12)
$H^\bullet + O_2^{\bullet-} \rightarrow HO_2^-$	(R13)
$HO_2^\bullet + O(^3P) \rightarrow O_2 + {}^\bullet OH$	(R14)
$H^+ + O_2^{\bullet-} \rightarrow HO_2^\bullet$	(R15)
$HO_2^\bullet \rightarrow H^+ + O_2^{\bullet-}$	
$O_2^{\bullet-} + H_2O \rightarrow HO_2^\bullet + OH^-$	(R16)
$HO_2^\bullet + OH^- \rightarrow O_2^{\bullet-} + H_2O$	

[a] O(^{3}P) denotes the oxygen atom in its ^{3}P ground state. [b] Reaction symbols used in the text.

TABLE 4: Main Track Reactions that Contribute to the Formation and Decay of H_2O_2 in Our Monte Carlo Simulations of the Radiolysis of Pure, Deaerated Liquid Water by 24 MeV $^{12}C^{6+}$ Ions (~500 KeV/μM) at 25 °C and in the Time Interval ~10^{-12}−10^{-6} s

reaction	symbol[a]
$^\bullet OH + {}^\bullet OH \rightarrow H_2O_2$	(R5)
$H^\bullet + HO_2^\bullet \rightarrow H_2O_2$	(R12)
$H_2O_2 + e_{aq}^- \rightarrow {}^\bullet OH + OH^-$	(R17)
$H^+ + HO_2^- \rightarrow H_2O_2$	(R18)
$H_2O_2 + OH^- \rightarrow HO_2^- + H_2O$	(R19)
$HO_2^- + H_2O \rightarrow H_2O_2 + OH^-$	

[a] Reaction symbols used in the text.

(~10^{-12}−10^{-6} s). Figures 4 and 5 compare, with and without multiple ionization of water, the time profiles of $\Delta G(HO_2^\bullet/O_2^{\bullet-})$ and $\Delta G(H_2O_2)$ of each of these reactions, respectively. As we can see in Figure 4, when the double, triple, and quadruple ionizations of water molecules are included in the simulations, $HO_2^\bullet/O_2^{\bullet-}$ is formed mainly by reactions R2, R10, R11, and R15, whereas its decay is dominated by reactions R6, R8, R12, and R14. The large increase in the fractions of $HO_2^\bullet/O_2^{\bullet-}$ formed by reactions R2, R10, and especially R11, compared to their corresponding values in the absence of multiple ionization, is a reflection of the large increase in the yields of O(^{3}P) and O_2 at high LET (see below). As regards H_2O_2, Figure 5 clearly demonstrates that H_2O_2 is formed within the tracks almost entirely by the reaction R5 of the $^\bullet$OH radical with itself, with or without multiple ionizations of water. However, our simulation results show that, upon incorporation of the multiple-ionization mechanism, the formation of H_2O_2 due to reaction R5 decreases. As noted above, this is explained by the fact that, in ~500 keV/μm $^{12}C^{6+}$ tracks, reactions R2, R6, and R7 compete with reaction R5, causing a decrease in the observed H_2O_2 yield (see Figure 3). Another reason for such a decrease in $G_{H_2O_2}$ arises from the decrease in the initial yield of $^\bullet$OH (at 10^{-13} s) due to the occurrence of reactions R1, R3, and R4, which do not produce $^\bullet$OH radicals, at the expense of the proton-transfer reaction $H_2O^{\bullet+} + H_2O \rightarrow H_3O^+ + {}^\bullet OH$, which occurs following the formation of singly ionized water molecules. The contributions of the reactions R17 and R19 to the removal of H_2O_2 also decrease with including the multiple ionizations of water as a result of the decrease in the H_2O_2 yield. As for the

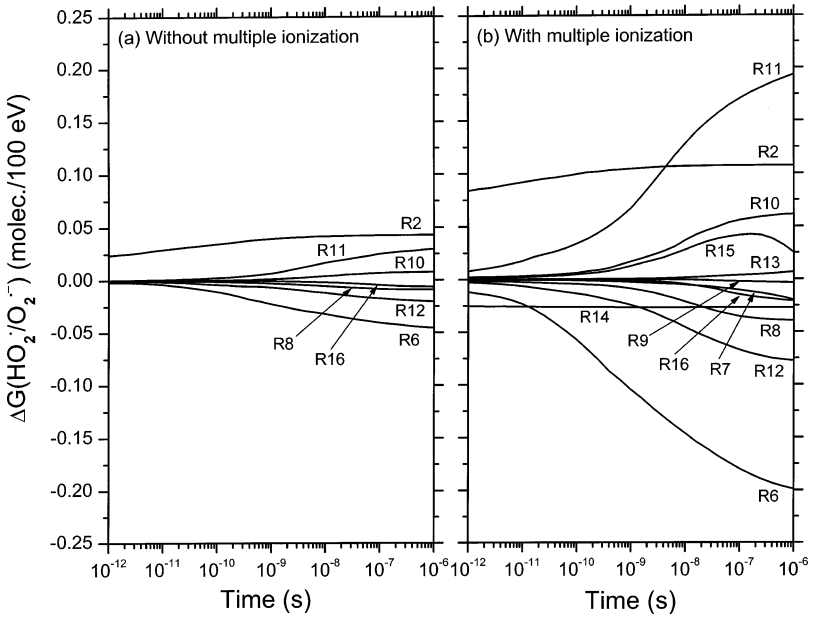

Figure 4. Time dependence of the extents $\triangle G(HO_2^{\bullet}/O_2^{\bullet-})$ (in molec./100 eV) of the main intratrack reactions R2 and R6−R16 that contribute to the formation and decay of $HO_2^{\bullet}/O_2^{\bullet-}$ (see text and Table 3), calculated from our Monte Carlo simulations of the radiolysis of deaerated liquid water by 24 MeV $^{12}C^{6+}$ ions (∼500 keV/μm) at neutral pH, 25 °C, and in the time interval $10^{-12}-10^{-6}$ s: (a) without including the mechanism of multiple ionization of water, and (b) with incorporating the double, triple, and quadruple ionizations of water molecules. Note that, in the absence of multiple ionization of water, the contributions of reactions R7, R9, and R13−R15 are very small and have been omitted from the figure for the sake of clarity.

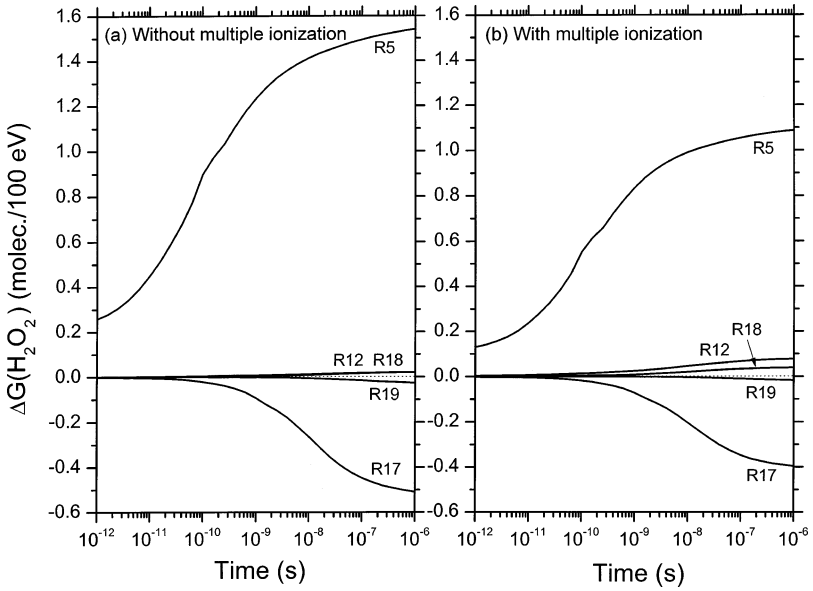

Figure 5. Time dependence of the extents $\triangle G(H_2O_2)$ (in molec./100 eV) of the main intratrack reactions R5, R12, and R17−R19 that are involved in the formation and decay of H_2O_2 (see text and Table 4) calculated from our Monte Carlo simulations of the radiolysis of deaerated liquid water by 24 MeV $^{12}C^{6+}$ ions (∼500 keV/μm) at neutral pH, 25 °C, and in the time interval $10^{-12}-10^{-6}$ s: (a) without including the mechanism of multiple ionization of water, and (b) with incorporating the double, triple, and quadruple ionizations of water molecules.

fractions of hydrogen peroxide formed by reactions R12 and R18, they are very small at the LET of ∼500 keV/μm considered here and show only little increase when multiple ionizations of water molecules are incorporated in the simulations, due to the increase in $HO_2^{\bullet}/O_2^{\bullet-}$ yields (see Figure 2). The net effects of multiple ionization of water on $G_{HO_2^{\bullet}/O_2^{\bullet-}}$ and $G_{H_2O_2}$ with increasing LET are shown in Figures 2 and 3, respectively.

The variations of $G_{e_{aq}^-}$ and $G^{\bullet}_{OH}$ (obtained at 10^{-6} s) as a function of LET for pure, deaerated liquid water irradiated by $^1H^+$, $^4He^{2+}$, $^{12}C^{6+}$, and $^{20}Ne^{9+}$ ions up to ∼900 keV/μm, at 25 °C, are shown in parts (a) and (b) of Figure 6, respectively. As can be seen, the primary yields of the hydrated electron and the hydroxyl radical diminish steeply as the LET is increased, and for the highest LET studied, there is almost no e_{aq}^- and $^{\bullet}OH$ surviving at the microsecond time scale. Also, for incident ions of equal LET, $G_{e_{aq}^-}$ and $G^{\bullet}_{OH}$ increase as the ion velocity increases, from protons to neon ions. This is as expected.[85] Figure 6 also shows that, for the range of LET considered here, the incorporation of multiple ionization of water in our simulations has almost no effect on $G_{e_{aq}^-}$ and $G^{\bullet}_{OH}$. In fact, our

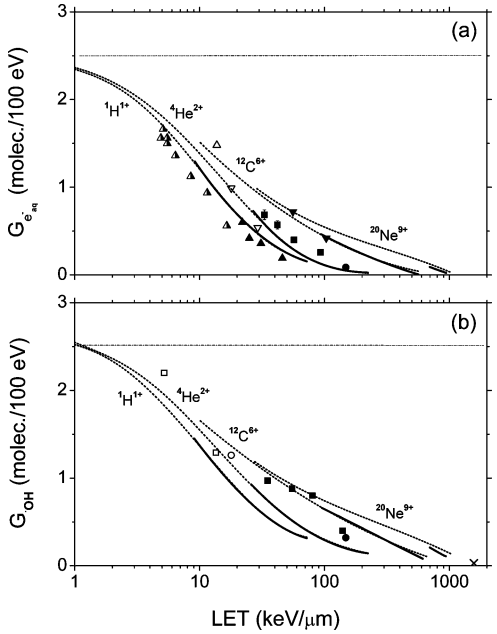

Figure 6. Variation of the primary yields of (a) hydrated electrons ($G_{e^-_{aq}}$) and (b) hydroxyl radicals ($G_{^\bullet OH}$) (in molec./100 eV) of the radiolysis of air-free liquid water by $^1H^+$, $^4He^{2+}$, $^{12}C^{6+}$, and $^{20}Ne^{9+}$ ions as a function of LET up to ~900 keV/μm, at neutral pH and 25°C. The solid lines represent the results of our Monte Carlo simulations incorporating the double, triple, and quadruple ionizations of water molecules, obtained at 10^{-6} s. The short-dot lines correspond to our results calculated without including the mechanism of multiple ionization of water. Experimental yields: (a) $^1H^+$ [(▽), ref 93], $^2H^+$, at one-half energy [(△), ref 15; (▲), ref 88], and $^4He^{2+}$ [(▼), ref 15; (●), ref 84; (▲), ref 88; (■), ref 94]; (b)$^1H^+$ [(□), ref 18; (○), ref 93], $^4He^{2+}$ [(■), ref 18; (●), ref 84], and $^{20}Ne^{9+}$ [(×), ref 18]. The dash−dot lines represent the limiting primary e^-_{aq} and $^\bullet OH$ yields obtained with ^{60}Co γ-rays or fast electrons (~2.5 molec./100 eV) (ref 11).

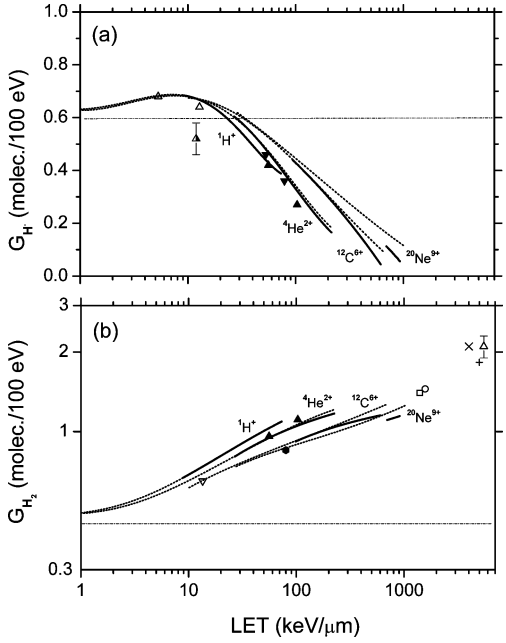

Figure 7. Variation of the primary yields of (a) hydrogen atoms ($G_{H^\bullet}$) and (b) molecular hydrogen (G_{H_2}) (in molec./100 eV) of the radiolysis of air-free liquid water by $^1H^+$, $^4He^{2+}$, $^{12}C^{6+}$, and $^{20}Ne^{9+}$ ions as a function of LET up to ~900 keV/μm, at neutral pH and 25°C. The solid lines represent the results of our Monte Carlo simulations incorporating the double, triple, and quadruple ionizations of water molecules, obtained at 10^{-6} s. The short-dot lines correspond to our results calculated without including the mechanism of multiple ionization of water. Experimental yields: (a) $^1H^+$ [(△), ref 95], $^2H^+$, at one-half energy [(▲), ref 83], and $^4He^{2+}$ [(▲), ref 15; (▼), ref 95]; (b) $^1H^+$ [(▽), ref 18], $^4He^{2+}$ [(▲), ref 15; (⬢), ref 18], $^{20}Ne^{5+}$ [(□), ref 96], $^{20}Ne^{9+}$ [(○), ref 18], and fission fragments [(×), ref 16; (+), ref 97; (△), ref 98]. The dash−dot lines represent the limiting primary $H^\bullet$ and H_2 yields obtained with ^{60}Co γ-rays or fast electrons (~0.60 and 0.45 molec./100 eV, respectively) (ref 2).

calculated yield values are nearly identical to those obtained without multiple ionization of water. Over the whole LET range, the simulations for the four ions are in quite good agreement with available experimental data.[15,18,84,88,93,94]

The effect of LET on $G_{H^\bullet}$ and G_{H_2} (obtained at 10^{-6} s) for pure, deaerated liquid water irradiated by $^1H^+$, $^4He^{2+}$, $^{12}C^{6+}$, and $^{20}Ne^{9+}$ ions up to ~900 keV/μm, at 25 °C, is shown in parts (a) and (b) of Figure 7, respectively. As one can see from Figure 7a, our calculated primary $H^\bullet$ atom yield values present a slight maximum near 6.5 keV/μm before decreasing steeply at higher LET. The origin of this maximum was discussed in detail previously.[99] Below ~10 keV/μm, the behavior of $G_{H^\bullet}$ is essentially independent of radiation quality. This is to be expected since in this low-LET region (that is, at high radiation particle energies), the tracks of heavy ions can be viewed, as seen above, as a random succession of (on average) isolated, nearly spherical spurs, and the observed chemistry of such particles should therefore be much like that of fast protons.[10,12] Our simulated results also show that, as do the yields of e^-_{aq} and $^\bullet OH$ (see Figure 6), for incident ions of a given LET > 10 keV/μm, $G_{H^\bullet}$ increases with ion velocity, from protons to neon ions.[85] In the LET range studied, our calculated $G_{H^\bullet}$ values are in good agreement with the experimental data of Appleby and Schwarz[15] and of Bisby et al.,[95] but are slightly higher than the $G_{H^\bullet}$ value determined by Elliot et al.[83] at room temperature for irradiations with a 23 MeV $^2H^+$ beam. It should be noted, however, that the $H^\bullet$ atom yield reported by these latter authors is estimated from the difference between the measured values of (G_{H_2} + $G_{H^\bullet}$) and G_{H_2}, and therefore has a rather large experimental uncertainty. As for our calculated primary H_2 yields, Figure 7b shows that they increase monotonically with increasing LET for the four impacting ions studied. For instance, in the case of deaerated liquid water irradiated by $^{12}C^{6+}$ ions, our computed G_{H_2} values are found to increase continuously from ~0.64 to 1.15 molec./100 eV on going from ~12 to 600 keV/μm. As can be seen, the available experimental data[15,18,96] are generally well reproduced by our calculated H_2 escape yields over the whole LET range covered here. However, extrapolation of our values to higher LET seems to be somewhat lower than the yield of ~2 molec./100 eV estimated for the decomposition of water by fission recoil fragments with an LET close to ~5000 keV/μm.[16,97,98] In view of the fact that the fission fragment data may have large uncertainties because of dosimetry,[11] further measurements of the H_2 yield using various ion types and ion energies over a wide range of LET values above ~100−200 keV/μm would be needed to clarify the results observed. Figure 7 also shows that, in the case of protons, the incorporation of the double, triple, and quadruple ionizations of water molecules in the simulations has no effect on the variations of $G_{H^\bullet}$ and G_{H_2} with LET. However, in the case of $^4He^{2+}$, $^{12}C^{6+}$, and $^{20}Ne^{9+}$ ions, we observe at high LET a slight gradual decrease of our $G_{H^\bullet}$ and G_{H_2} values calculated with multiple ionization of water in comparison with those obtained without including the multiple-ionization mechanism. This decrease of $G_{H^\bullet}$ and G_{H_2} at low ion energies is more pronounced for heavier ions in the order $^4He^{2+}$ < $^{12}C^{6+}$ < $^{20}Ne^{9+}$ and mainly results from the increase in the yields of $HO_2^\bullet/O_2^{\bullet-}$ and O_2 (see

below) that occurs at high LET in the presence of the multiple ionization of water. In the case of H_2, for example, the main reactions that account for its formation in pure, deaerated liquid water irradiated with ~500 keV/μm $^{12}C^{6+}$ ions are, in order of decreasing importance (data not shown):

$$H^{\bullet} + e_{aq}^{-} \rightarrow H_2 + OH^{-} \qquad \text{(R20)}$$

$$e_{aq}^{-} + e_{aq}^{-} \rightarrow H_2 + 2OH^{-} \qquad \text{(R21)}$$

and

$$H^{\bullet} + H^{\bullet} \rightarrow H_2 \qquad \text{(R22)}$$

As $H^{\bullet}$ reacts with O_2 and $HO_2^{\bullet}/O_2^{\bullet-}$ in the dense $^{12}C^{6+}$ ion tracks by reactions R11−R13 (see Table 3 and Figures 4 and 5), these reactions normally compete with reactions R20 and R22 at early time and during track expansion, thereby causing a decrease in the observed H_2 yield at high LET. For the example under consideration, the overall variation of G_{H_2} with and without incorporation of multiple ionization of water is $\Delta G(H_2) \approx -0.07$ molec./100 eV at 10^{-6} s (data not shown).

Oxygen is a powerful radiation sensitizer.[100] The biological response to irradiation is greater under oxygenated conditions than under hypoxic conditions. The ratio of hypoxic to aerated doses needed to achieve the *same* biological effect is known as the "oxygen enhancement ratio" (OER). The OER is generally recognized as a dose-modifying factor of fundamental importance in radiobiology as well as of practical importance in radiotherapy. For most cellular organisms, it is well established that the value of OER decreases progressively with increasing LET of the radiation.[101,102] The "oxygen-in-the-track" hypothesis, proposed many years ago to account for this effect,[103] presupposes that molecular oxygen is a product of the radiolysis of water at high LET. In fact, the radiolytic formation of O_2 in the tracks of highly charged particles is presumed to convert an initially "hypoxic" solution to a partially "oxygenated" microenvironment around the relevant cellular target molecules, which justifies the low OER values observed in the experiments.[17,102,104] This hypothesis of the generation of molecular oxygen in heavy-ion tracks has often been invoked for a variety of biological materials, but the conclusion is not clear yet.[105] On the viewpoint of pure radiation chemistry, the creation of O_2 along the tracks of highly charged particles has been proposed by several studies.[16,17,20,106−109] Those measurements all support the proposal that track oxygen is a product of the radiolysis of water at high LET. Most remarkably, Bibler[16] estimated from his studies of the radiolysis of 0.4 M H_2SO_4 solutions with ^{252}Cf fission fragments that G_{O_2} could be as large as ~0.8 molec./100 eV at an LET of ~4000 keV/μm (to make up the material balance).

In the present work, upon incorporation of the double, triple, and quadruple ionizations of water molecules in our simulations of the radiolysis of pure, deaerated liquid water, we find, for the four irradiating ions used ($^1H^+$, $^4He^{2+}$, $^{12}C^{6+}$, and $^{20}Ne^{9+}$), a steep increase in both the initial (at 10^{-13} s) (Figure 8a) and the primary (at 10^{-6} s) (Figure 8b) yields of O_2 as a function of LET. In contrast, in the absence of the multiple ionization of water, these yields remain very small throughout the range of LET studied and show only a slight gradual increase with increasing LET. It is difficult, unfortunately, to offer a quantitative comparison between our calculated initial *G*-values for molecular oxygen and the corresponding experimental data of Baverstock and Burns.[17] In fact, the latter authors obtained, for several different impacting ions, the initial yields of O_2 as the lowest limiting yields when the concentration of Fe^{2+} ions was increased (usually to 10^{-2}−10^{-1} M) in deaerated Fricke dosimeter solutions (10^{-3} M ferrous ammonium sulfate in aqueous 0.4 M H_2SO_4) (Table 1 of ref 17). However, they subsequently showed in more detailed experiments using higher ferrous ion concentrations[108] that, with increasing concentration of Fe^{2+} ions, the observed yield of oxygen passes through a minimum, which is dependent upon LET, and rises thereafter. It is clear, under such circumstances, that the initial yields of track oxygen reported by Baverstock and Burns[17] are certainly subject to large uncertainty on an absolute basis. We note, nevertheless, that the initial $G(O_2)$ value (~0.005 molec./100 eV) that these authors estimated for 5 MeV $^4He^{2+}$ ions (LET ~90 keV/μm)[17] agrees very well with our calculated value of 0.0064 molec./100 eV (Figure 8a). However, for 30 MeV $^{20}Ne^{9+}$ ions (LET ~1570 keV/μm),[17,108] their observed initial O_2 yield (0.031 molec./100 eV) is about a factor of 10 smaller than our calculated value (~0.3 molec./100 eV, obtained by extrapolation of the data of Figure 8a). As opposed to the difficulties encountered with the initial O_2 yields, a reliable quantitative comparison of our simulated results for ($G_{HO_2^{\bullet}/O_2^{\bullet-}} + G_{O_2}$) as a function of LET (Figures 2 and 8b) can be made with experiment,[17−20,108] *bearing in mind that the yields generally quoted for $HO_2^{\bullet}$ in the literature also include O_2 as a direct radiolysis product*.[11,17] For instance, for ~140 keV/μm $^4He^{2+}$ ions, Figures 2 and 8b (when the mechanism of multiple ionization of water is included in the calculations) give $G_{HO_2^{\bullet}/O_2^{\bullet-}} = 0.046$ molec./100 eV and $G_{O_2} = 0.034$ molec./

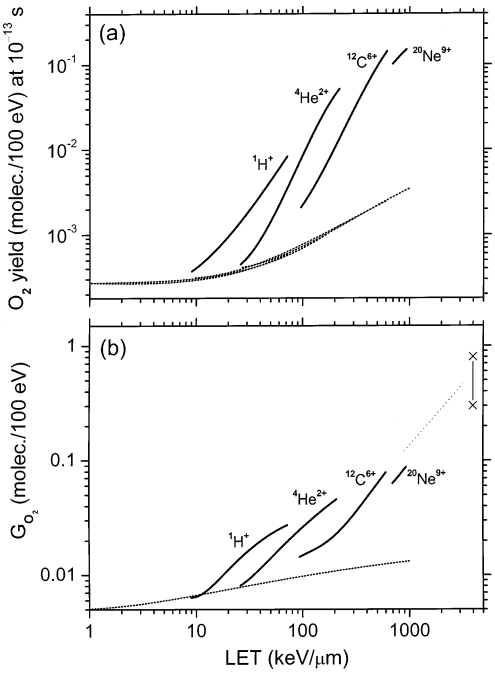

Figure 8. Variation of the initial (a) and primary (b) yields of molecular oxygen (obtained at 10^{-13} and 10^{-6} s, respectively) (in molec./100 eV) of the radiolysis of liquid water by $^1H^+$, $^4He^{2+}$, $^{12}C^{6+}$, and $^{20}Ne^{9+}$ ions as a function of LET, at neutral pH and 25°C. The solid lines represent the results of our Monte Carlo simulations incorporating the double, triple, and quadruple ionizations of water molecules. The short-dot lines correspond to our calculated values without including the mechanism of multiple ionization of water. The yields $G_{O_2} \sim 0.3$ and 0.8 molec./100 eV estimated by Bibler (ref 16) (×) in the ^{252}Cf fission fragment radiolysis of 0.4 M H_2SO_4 solutions at very high LET (~4000 keV/μm) are also shown in part (b) of the figure. The dot line is drawn here as a guide for the eye to show that extrapolation to higher LET of our calculated O_2 escape yields for the four ions studied reproduces well Bibler's estimates.

TABLE 5: Main Track Reactions that Contribute to the Formation and Decay of O_2 in Our Monte Carlo Simulations of the Radiolysis of Pure, Deaerated Liquid Water by 24 MeV $^{12}C^{6+}$ Ions (~500 KeV/μM) at 25 °C and in the Time Interval $\sim 10^{-12}-10^{-6}$ s

reaction	symbol[a]
$^{\bullet}OH + HO_2^{\bullet} \rightarrow O_2 + H_2O$	(R6)
$^{\bullet}OH + O_2^{\bullet -} \rightarrow O_2 + OH^-$	(R7)
$e_{aq}^- + O_2 \rightarrow O_2^{\bullet -}$	(R10)
$H^{\bullet} + O_2 \rightarrow HO_2^{\bullet}$	(R11)
$HO_2^{\bullet} + O(^3P) \rightarrow O_2 + {}^{\bullet}OH$	(R14)
$O(^3P) + O(^3P) \rightarrow O_2$	(R21)

[a] Reaction symbols used in the text.

100 eV, respectively, so that $(G_{HO_2^{\bullet}/O_2^{\bullet -}} + G_{O_2}) = 0.08$ molec./100 eV. This value reproduces very well the corresponding experimental values of 0.08 (Table 1 of ref 17), 0.085,[18] 0.099,[19−20] and ~0.093[108] molec./100 eV. It is also consistent with other experimental data at similar or slightly lower LET, including those of Lefort and Tarrago[14] (0.11 molec./100 eV) and Senvar and Hart[110] (0.10 molec./100 eV) for 5.3 MeV and 3.4 MeV ^{210}Po α particles, respectively, and of Appleby and Schwarz[15] (0.07 molec./100 eV) for 12 MeV $^4He^{2+}$ ions. The same kind of comparison can be done at higher LET, for example for $^{20}Ne^{9+}$ ions at ~1570 keV/μm. By extrapolation of our results of Figures 2 and 8b, we obtain for this case $G_{HO_2^{\bullet}/O_2^{\bullet -}} \approx 0.11$ molec./100 eV and $G_{O_2} \approx 0.17$ molec./100 eV, so that $(G_{HO_2^{\bullet}/O_2^{\bullet -}} + G_{O_2}) \approx 0.28$ molec./100 eV. This value is in quite good agreement with the corresponding measured yields of 0.25,[17,108] 0.27,[18] and 0.24[19−20] molec./100 eV reported in the literature for $^{20}Ne^{9+}$ ions at this particular LET. This good agreement between calculated and experimental yield values gives strong support to the validity and consistency of the model,[111] and in turn to the importance of the role of multiple ionization in the radiolysis of water under high-LET irradiation conditions. A final remark that is worthwhile to mention here concerns the relative yields of $HO_2^{\bullet}/O_2^{\bullet -}$ and O_2 in the tracks of highly charged particles. As can be seen from Figures 2 and 8b, not only does the sum $(G_{HO_2^{\bullet}/O_2^{\bullet -}} + G_{O_2})$ increase with increasing LET but also the amount of O_2 produced, which is low at low LET, becomes greater than that of $HO_2^{\bullet}/O_2^{\bullet -}$ for very high-LET ions. In fact, using the same examples as those cited just above, the ratio $G_{O_2}:G_{HO_2^{\bullet}/O_2^{\bullet -}}$ is calculated to increase from about 0.73 to 1.55 as the LET is raised from ~140 to 1570 keV/μm. These results clearly demonstrate the usefulness of the present computer simulation studies to elucidate the problem of the separation of the combined yields of $HO_2^{\bullet}$ and O_2 in high-LET heavy-ion radiolysis experiments using deaerated Fe^{2+}/Cu^{2+} aqueous solutions under acidic conditions.[109]

Further insights into the effects of multiple ionization of water on G_{O_2} in the heavy-ion water radiolysis can be gained by examining the unfolding of the various reactions that contribute to the formation or decay of O_2 in the ion tracks as they expand by diffusion. The main reactions that are involved in the primary yield of O_2 in the case of deaerated liquid water irradiated by 24 MeV $^{12}C^{6+}$ ions (~500 keV/μm) at neutral pH and 25 °C are listed in Table 5. As noted above, the importance of these reactions can be quantified by the yield variations $\Delta G(O_2)$ that they cause over the time interval of nonhomogeneous track chemistry ($\sim 10^{-12}-10^{-6}$ s). In Figure 9, we compare, with and without including the mechanism of multiple ionization of water, our calculated time profiles of $\Delta G(O_2)$ for each of these reactions. Figure 9a shows that, in the absence of multiple ionization, the production and disappearance of molecular oxygen are predominantly due to intratrack reactions R6 and R7, and R10 and R11, respectively. Overall, the amount of O_2 produced is slightly larger than that removed, so that our calculated G_{O_2} value at the microsecond time scale is low (~0.013 molec./100 eV; see Figures 8b and 10a). When the double, triple, and quadruple ionizations of water molecules are incorporated in the simulations (Figure 9b), O_2 is formed within the tracks mainly by reaction R6 and to a much lower extent by reaction R7, whereas there is a chemical production of O_2 at early times originating from the reactions R14 and R21 of the $O(^3P)$ atom[112] with $HO_2^{\bullet}$ and with itself, respectively. As for the O_2 decay, it largely occurs through the two track reactions R10 and especially R11. Compared to the results obtained in the absence of multiple ionization, there is overall a marked (about five times) increase in the production of O_2 over its disappearance, our calculated value of G_{O_2} being equal, in this case, to ~0.062 molec./100 eV (see Figures 8b and 10b). A detailed inspection of Figure 9 also reveals the presence of a maximum in the time dependence of the O_2 yield (Figure 10), which is mainly accounted for by the different formation and decay kinetics of molecular oxygen. In fact, reaction R6, which is the dominant chemical route for formation of O_2, takes place at very short times and its importance in producing O_2 increases rapidly around $\sim 10^{-11}$ s. By contrast, the reactions R10 and R11, which are the principal causes of the decay of O_2, show a comparatively slower initial increase in importance, but this trend is reversed on the time scale from $\sim 10^{-10}$ to 10^{-9} s with an increasingly faster decay of O_2. This leads, in turn, to the appearance of a maximum in the O_2 yield at around 10^{-9} s. As it is clearly seen in Figure 10, for 24 MeV $^{12}C^{6+}$ ions (~500 keV/μm), this maximum is very shallow in the absence of the multiple-ionization mechanism, but becomes quite pronounced (~0.13 molec./100 eV at $\sim 4 \times 10^{-10}$ s) when the double, triple, and quadruple ionizations of water molecules are incorporated in the simulations.

Parts (a) and (b) of Figure 10 show the effect of LET on the temporal variation of the yield of O_2 at 25 °C, over the range $10^{-12}-10^{-6}$ s, obtained from our simulations of the radiolysis of pure, deaerated liquid water by $^{12}C^{6+}$ ions of various initial energies in the range ~18−2 MeV/nucleon (~100−500 keV/μm). As can be seen from Figures 9a and 10a, in the absence of multiple ionization of water, the initial yield of molecular oxygen is almost nonexistent for all LET values considered, while at longer times there is a small amount of O_2 produced via intratrack reactions occurring during the nonhomogeneous chemical stage. In contrast, upon incorporation of multiple ionization of water molecules in our simulations, the production of O_2 increases considerably with increasing LET.[113] Figures 9b and 10b demonstrate that, in this case, the amount of O_2 produced by the very short-time track reactions R6, R14, and R21 is the primary cause of the overall increase in the yield of O_2. The results in Figure 10b also show that, as the LET is increased, the maximum of the O_2 yield becomes more and more pronounced as a function of time, while its position continuously shifts toward shorter times. Unfortunately, there is at present no experimental or theoretical information available in the literature with which to compare our results on the time variations of the yield of molecular oxygen at high LET.

A few final words should be added here regarding the oxygen production in high-LET ion tracks. Using our calculated G values for O_2 reported above for 24 MeV $^{12}C^{6+}$ ions (~500 keV/μm) (see Figures 8a and 10b), we can estimate the track concentration of O_2 as a function of time. In fact, assuming that the oxygen molecules are produced *evenly* in a cylinder

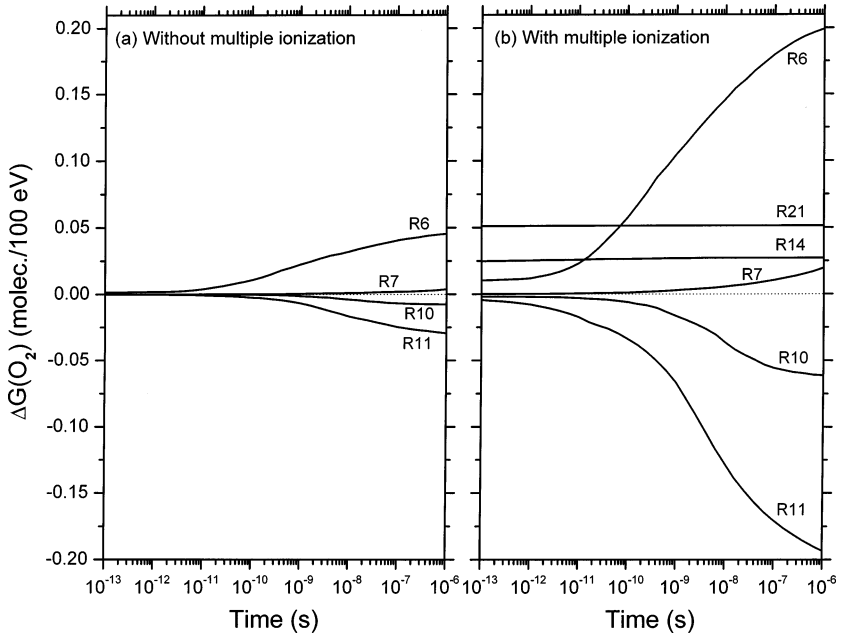

Figure 9. Time dependence of the extents $\triangle G(O_2)$ (in molec./100 eV) of the main intratrack reactions R6, R7, R10, R11, R14, and R21 that contribute to the formation and decay of molecular oxygen (see text and Table 5), calculated from our Monte Carlo simulations of the radiolysis of deaerated liquid water by 24 MeV $^{12}C^{6+}$ ions (~500 keV/μm) at neutral pH, 25 °C, and in the time interval $10^{-12}-10^{-6}$ s: (a) without including the mechanism of multiple ionization of water, and (b) with incorporating the double, triple, and quadruple ionizations of water molecules. Note that, in the absence of multiple ionization of water, the contributions of reactions R14 and R21 are very small and have been omitted from the figure for the sake of clarity.

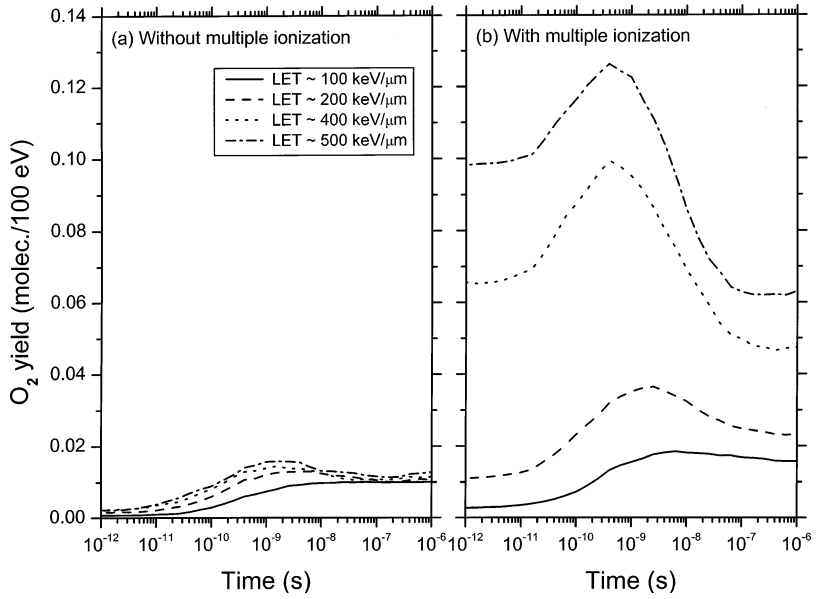

Figure 10. Time dependences of the O_2 yields (in molec./100 eV) calculated from our Monte Carlo simulations of the radiolysis of pure, deaerated liquid water at neutral pH, 25 °C, and in the time scale of $10^{-12}-10^{-6}$ s, for impacting $^{12}C^{6+}$ ions of various initial energies: 18 (~100 keV/μm), 8 (~200 keV/μm), 3 (~400 keV/μm), and 2 (~500 keV/μm) MeV/nucleon (see text), without mutiple ionization of water (a), and with including the double, triple, and quadruple ionizations of water molecules (b).

whose initial radius r_0 is equal to the radius of the physicochemical core of the impacting ion track (at 10^{-13} s),[8,9] this concentration can simply be derived from[2,17,56]

$$[O_2] \approx G(O_2) \times \left(\frac{LET}{\pi r(t)^2}\right)$$

where

$$r(t)^2 \approx r_0^2 + 6Dt$$

represents the change with time of r_0 due to the diffusive expansion of the track. Here, t is the time and D is the diffusion coefficient of O_2 ($D = 2.42 \times 10^{-9}$ m^2 s^{-1} at 25 °C).[50] For the case of 24 MeV $^{12}C^{6+}$ ions, the LET is ~500 keV/μm, $G(O_2)$ at 10^{-13} s is ~0.1 molec./100 eV (Figure 8a), and r_0 obtained from our simulations is ~2.0 nm. Under these conditions, the initial track concentration of oxygen $[O_2]_0$ is ~63.5 mM, a value that is about 3 orders of magnitude higher than the concentration of O_2 found in typical human cells (~30 μM).[114] At ~4×10^{-10} s (that is, at the O_2 yield maximum; see Figure 10b), we have

$r \sim 3.1$ nm, $G(O_2) \sim 0.13$ molec./100 eV, and thus $[O_2] \sim 32.8$ mM. Finally, at the microsecond time scale, $r \sim 121$ nm, $G_{O_2} \sim 0.063$ molec./100 eV, and the oxygen concentration in the irradiated track volume is ~ 11 μM. All of these values clearly indicate that there is an excess production in situ of molecular oxygen in high-LET, heavy-ion tracks at early time that is not observed with lower LET radiations. One must nevertheless be cautious in relating these substantial O_2 yields and concentrations, which are for water, to the situation where energy is deposited in or near a cell.[105] However, it seems certain that this O_2 formation can be an important factor in the increased biological efficiency of radiations of high LET with, in turn, profound consequences in radiobiology, oxidative processes, and other applications. In view of the above results, the present work largely pleads in favor of the "oxygen in the heavy-ion track" hypothesis.

4. Conclusion

In this study, we have used Monte Carlo track structure simulations to investigate the effects of multiple ionization of water on the *G*-values of the radiolytic free radical and molecular species, including O_2, produced in the radiolysis of pure, air-free liquid water by several different types of radiation, including $^1H^+$, $^4He^{2+}$, $^{12}C^{6+}$, and $^{20}Ne^{9+}$ ions, at high LET up to $\sim$900 keV/μm, at neutral pH and 25 °C. Taking into account the double, triple, and quadruple ionizations of water molecules, the primary (or "escape") yields $G_{HO_2^\bullet/O_2^{\bullet-}}$, $G_{H_2O_2}$, $G_{e^-_{aq}}$, $G_{^\bullet OH}$, $G_{H^\bullet}$, G_{H_2}, and G_{O_2}, have been calculated as a function of LET. A good agreement has been obtained between the calculated yields and the available experimental data. In particular, our results quantitatively reproduce the large increase observed in the $HO_2^\bullet/O_2^{\bullet-}$ yield with increasing LET. With the exception of protons, they also simultaneously predict a maximum in the yield of H_2O_2 around 100−200 keV/μm in remarkable accord with experiment. In addition, for each ion investigated, this maximum of $G_{H_2O_2}$ occurs precisely at the point where $G_{HO_2^\bullet/O_2^{\bullet-}}$ begins to rise sharply, showing, in agreement with previous experimental data, that the yields of $HO_2^\bullet/O_2^{\bullet-}$ and H_2O_2 are closely linked. However, we find that, over the whole LET range considered, the incorporation of multiple ionization of water in the simulations has almost no effect on the variation of our computed $G_{e^-_{aq}}$ and $G_{^\bullet OH}$ values. It is also found that $G_{e^-_{aq}}$ and $G_{^\bullet OH}$ diminish steeply as the LET is increased; for the highest LET studied, there is almost no escape of e^-_{aq} and $^\bullet OH$ from the ion track at the microsecond time scale. In contrast, we observe for $^4He^{2+}$, $^{12}C^{6+}$, and $^{20}Ne^{9+}$ ions at high LET a slight gradual decrease of our $G_{H^\bullet}$ and G_{H_2} values calculated with multiple ionization of water in comparison with those obtained without including the multiple-ionization mechanism. This decrease of $G_{H^\bullet}$ and G_{H_2} at low ion energies is found to be more pronounced for heavier ions in the order $^4He^{2+} < {}^{12}C^{6+} < {}^{20}Ne^{9+}$ and mainly results from the increase in $HO_2^\bullet/O_2^{\bullet-}$ and O_2 yields that occurs at high LET in the presence of the multiple ionization of water. As expected, $G_{H^\bullet}$ at first increases and then decreases at high LET, whereas G_{H_2} monotonically rises with increasing LET. For the four irradiating ions used, our results also show, upon incorporation of multiple ionization of water molecules in the simulations, a steep increase in both the initial (at 10^{-13} s) and the primary (at 10^{-6} s) yields of O_2 as a function of LET. Moreover, detailed examination of the temporal variation of the yield of O_2 reveals the presence of a maximum at around 10^{-9} s. For 24 MeV $^{12}C^{6+}$ ions ($\sim$500 keV/μm), this maximum is very shallow in the absence of the multiple-ionization mechanism, but reaches a value of $\sim$0.13 molec./100 eV when the double, triple, and quadruple ionizations of water molecules are incorporated in the simulations. Such an excess production in situ of molecular oxygen in high-LET, heavy-ion tracks, that is not observed with lower LET radiations, can be a key factor in the increased biological efficiency of radiations of high LET with, in turn, important consequences in radiobiology, oxidative processes, and other applications. Based on these results, the present work clearly pleads in favor of the "oxygen in the heavy-ion track" hypothesis. Finally, it is worthwhile noting that, under the conditions of this study, the mechanisms of triple and quadruple ionizations contribute only weakly to the production of $HO_2^\bullet/O_2^{\bullet-}$ and O_2, respectively. In other words, the mechanism of double ionization of water is found to largely predominate at high LET, whereas it is insignificant at low LET.

The good overall agreement found between calculated and experimental yield values gives strong support to the validity and consistency of the model used in this study, and in turn to the importance of the role of multiple ionization in the radiolysis of water under high-LET irradiation conditions.

Acknowledgment. We are grateful to Professor Hans Bichsel, Dr. Christophe Champion, Professor Yosuke Katsumura, Professor Jay A. LaVerne, Dr. John H. Miller, Professor Dr. Clemens von Sonntag, and Professor David E. Watt for valuable discussions and useful correspondence, and to Mr. Carol Gauthier for his skillful assistance with the computer programs. We would also like to thank the "Réseau québécois de calcul de haute performance" (RQCHP) for providing generous computing facilities. Financial support from the Canadian Institutes of Health Research (Grant No. MT-14617) and the Natural Sciences and Engineering Research Council of Canada (Grant No. 9020-04) is gratefully acknowledged.

References and Notes

(1) Spinks, J. W. T.; Woods, R. J. *An Introduction to Radiation Chemistry*, 3rd ed.; Wiley: New York, 1990; p 243.
(2) Ferradini, C.; Jay-Gerin, J.-P. *Can. J. Chem.* **1999**, *77*, 1542.
(3) Buxton, G. V. In *Charged Particle and Photon Interactions with Matter. Chemical, Physicochemical, and Biological Consequences with Applications*; Mozumder, A., Hatano, Y., Eds.; Marcel Dekker: New York, 2004; p 331.
(4) Magee, J. L. *Annu. Rev. Nucl. Sci.* **1953**, *3*, 171.
(5) See, for example: Plante, I. L.; Filali-Mouhim, A.; Jay-Gerin, J.-P. *Radiat. Phys. Chem.* **2005**, *72*, 173.
(6) Throughout this paper, radiation chemical yields (*G*-values) are given in the units of molecules per 100 eV (molec./100 eV). For conversion into SI units (mol/J): 1 molec./100 eV $\approx$ 0.10364 μmol/J.
(7) Ferradini, C. *J. Chim. Phys.* **1979**, *76*, 636.
(8) Magee, J. L.; Chatterjee, A. In *Kinetics of Nonhomogeneous Processes*; Freeman, G. R., Ed.; Wiley: New York, 1987; p 171.
(9) Mozumder, A. *Fundamentals of Radiation Chemistry*; Academic Press: San Diego, CA, 1999.
(10) LaVerne, J. A. *Radiat. Res.* **2000**, *153*, 487.
(11) LaVerne, J. A. In *Charged Particle and Photon Interactions with Matter. Chemical, Physicochemical, and Biological Consequences with Applications*; Mozumder, A., Hatano, Y., Eds.; Marcel Dekker: New York, 2004; p 403.
(12) Appleby, A. *Radiat. Phys. Chem.* **1989**, *34*, 121.
(13) Note that, for low-LET radiolysis, the production of $HO_2^\bullet/O_2^{\bullet-}$ is usually neglected because its very small yield of $\sim$0.02 molec./100 eV (see: Bjergbakke, E.; Hart, E. J. *Radiat. Res.* **1971**, *45*, 261) accounts for less than 1% of the other primary radiolytic species.
(14) Lefort, M.; Tarrago, X. *J. Phys. Chem.* **1959**, *63*, 833.
(15) Appleby, A.; Schwarz, H. A. *J. Phys. Chem.* **1969**, *73*, 1937. Schwarz, H. A.; Caffrey, J. M., Jr.; Scholes, G. *J. Am. Chem. Soc.* **1959**, *81*, 1801.
(16) Bibler, N. E. *J. Phys. Chem.* **1975**, *79*, 1991.
(17) Baverstock, K. F.; Burns, W. G. *Nature* **1976**, *260*, 316.
(18) Burns, W. G.; Sims, H. E. *J. Chem. Soc., Faraday Trans. 1* **1981**, *77*, 2803. See also: Sims, H. E. Ph.D. Thesis, University of Salford, Salford, U.K., 1978.
(19) LaVerne, J. A.; Schuler, R. H.; Burns, W. G. *J. Phys. Chem.* **1986**, *90*, 3238.

(20) LaVerne, J. A.; Schuler, R. H. *J. Phys. Chem.* **1987**, *91*, 6560.

(21) Baldacchino, G.; Le Parc, D.; Hickel, B.; Gardès-Albert, M.; Abedinzadeh, Z.; Jore, D.; Deycard, S.; Bouffard, S.; Mouton, V.; Balanzat, E. *Radiat. Res.* **1998**, *149*, 128.

(22) McCracken, D. R.; Tsang, K. T.; Laughton, P. J. *Aspects of the Physics and Chemistry of Water Radiolysis by Fast Neutrons and Fast Electrons in Nuclear Reactors*, Report AECL-11895; Atomic Energy of Canada Limited: Chalk River, Ontario, 1998.

(23) Pastina, B.; LaVerne, J. A. *J. Phys. Chem. A* **1999**, *103*, 1592.

(24) Meesungnoen, J.; Filali-Mouhim, A.; Snitwongse Na Ayudhya, N.; Mankhetkorn, S.; Jay-Gerin, J.-P. *Chem. Phys. Lett.* **2003**, *377*, 419.

(25) Ferradini, C.; Jay-Gerin, J.-P. *Radiat. Phys. Chem.* **1998**, *51*, 263.

(26) It is worth noting here that a similar conclusion was pointed out more than fifty years ago by Platzman (Platzman, R. L. In *Symposium on Radiobiology. The Basic Aspects of Radiation Effects on Living Systems*; Nickson, J. J., Ed. Wiley: New York, 1952; p 97) in a discussion of the possible role of multiple ionization in radiation action.

(27) Champion, C. *Nucl. Instrum. Methods Phys. Res. B* **2003**, *205*, 671.

(28) Cobut, V.; Frongillo, Y.; Patau, J. P.; Goulet, T.; Fraser, M.-J.; Jay-Gerin, J.-P. *Radiat. Phys. Chem.* **1998**, *51*, 229.

(29) Frongillo, Y.; Goulet, T.; Fraser, M.-J.; Cobut, V.; Patau, J. P.; Jay-Gerin, J.-P. *Radiat. Phys. Chem.* **1998**, *51*, 245.

(30) Hervé du Penhoat, M.-A.; Goulet, T.; Frongillo, Y.; Fraser, M.-J.; Bernat, Ph.; Jay-Gerin, J.-P. *J. Phys. Chem. A* **2000**, *104*, 11757. See also: Hervé du Penhoat, M.-A.; Meesungnoen, J.; Goulet, T.; Filali-Mouhim, A.; Mankhetkorn, S.; Jay-Gerin, J.-P. *Chem. Phys. Lett.* **2001**, *341*, 135.

(31) Meesungnoen, J.; Benrahmoune, M.; Filali-Mouhim, A.; Mankhetkorn, S.; Jay-Gerin, J.-P. *Radiat. Res.* **2001**, *155*, 269.

(32) Muroya, Y.; Meesungnoen, J.; Jay-Gerin, J.-P.; Filali-Mouhim, A.; Goulet, T.; Katsumura, Y.; Mankhetkorn, S. *Can. J. Chem.* **2002**, *80*, 1367.

(33) Michaud, M.; Wen, A.; Sanche, L. *Radiat. Res.* **2003**, *159*, 3.

(34) Goulet, T.; Jay-Gerin, J.-P.; Frongillo, Y.; Cobut, V.; Fraser, M.-J. *J. Chim. Phys.* **1996**, *93*, 111.

(35) Bartels, D. M.; Cook, A. R.; Mudaliar, M.; Jonah, C. D. *J. Phys. Chem. A* **2000**, *104*, 1686.

(36) Muroya, Y.; Lin, M.; Wu, G.; Iijima, H.; Yoshii, K.; Ueda, T.; Kudo, H.; Katsumura, Y. *Radiat. Phys. Chem.* **2005**, *72*, 169.

(37) Pimblott, S. M.; LaVerne, J. A.; Bartels, D. M.; Jonah, C. D. *J. Phys. Chem.* **1996**, *100*, 9412.

(38) Pastina, B.; LaVerne, J. A.; Pimblott, S. M. *J. Phys. Chem. A* **1999**, *103*, 5841.

(39) Schwarz, H. A. *J. Phys. Chem.* **1969**, *73*, 1928.

(40) LaVerne, J. A.; Pimblott, S. M. *J. Phys. Chem.* **1991**, *95*, 3196.

(41) Subexcitation electrons are those that have kinetic energies lower than the first electronic excitation threshold of the medium (∼7.3 eV in liquid water, see: Michaud, M.; Cloutier, P.; Sanche, L. *Phys. Rev. A* **1991**, *44*, 5624). They lose energy relatively slowly, the dominant mode of energy loss being the excitation of molecular vibrations. See, for example, ref 9.

(42) Goulet, T.; Patau, J. P.; Jay-Gerin, J.-P. *J. Phys. Chem.* **1990**, *94*, 7312; *Radiat. Prot. Dosim.* **1990**, *31*, 33.

(43) Pimblott, S. M.; LaVerne, J. A. *J. Phys. Chem. A* **1997**, *101*, 5828.

(44) Pimblott, S. M.; Mozumder, A. In *Charged Particle and Photon Interactions with Matter. Chemical, Physicochemical, and Biological Consequences with Applications*; Mozumder, A., Hatano, Y., Eds.; Marcel Dekker: New York, 2004; p 75.

(45) Our average electron thermalization distance of ∼11.7 nm should be compared with $\langle r \rangle = 2\sqrt{2}\,\sigma/\sqrt{\pi}$, where σ is the width of the three-dimensional Gaussian distribution that describes the local spatial distribution of e_{aq}^- in deterministic "average" spur models of liquid water radiolysis by low-LET radiation (see: Goulet, T.; Jay-Gerin, J.-P. *Radiat. Res.* **1989**, *118*, 46). Most recent estimations of σ are 4−5 nm (refs 10 and 43) and 5.2 nm (ref 44). This relatively large average electron thermalization distance value comes from the presence of a long tail in our simulated distribution of thermalization distances, which indicates that a number of electrons travel large distances (up to ∼40 nm) from subexcitation to thermal energies (refs 28 and 34).

(46) Bartels, D. M.; Gosztola, D.; Jonah, C. D. *J. Phys. Chem. A* **2001**, *105*, 8069.

(47) Cobut, V.; Jay-Gerin, J.-P.; Frongillo, Y.; Patau, J. P. *Radiat. Phys. Chem.* **1996**, *47*, 247.

(48) Melton, C. E. *J. Chem. Phys.* **1972**, *57*, 4218.

(49) Severs, J. C.; Harris, F. M.; Andrews, S. R.; Parry, D. E. *Chem. Phys.* **1993**, *175*, 467.

(50) *CRC Handbook of Chemistry and Physics*, 84th ed.; Lide, D. R., Ed.; CRC Press: Boca Raton, FL, 2003.

(51) Rudd, M. E. *Radiat. Prot. Dosim.* **1990**, *31*, 17. See also: Rudd, M. E.; Kim, Y.-K.; Madison, D. H.; Gay, T. J. *Rev. Mod. Phys.* **1992**, *64*, 441.

(52) See, for example: ICRU Report 55. *Secondary Electron Spectra from Charged Particle Interactions*; International Commission of Radiation Units and Measurements: Bethesda, MD, 1996. Inokuti, M. *Rev. Mod. Phys.* **1971**, *43*, 297.

(53) LaVerne, J. A. *Radiat. Phys. Chem.* **1989**, *34*, 135.

(54) The principle of this method to measure $HO_2^\bullet$ is to generate molecular oxygen by the reaction of $HO_2^\bullet$ with cupric ion (see: Hart, E. J. *Radiat. Res.* **1955**, *2*, 33. Donaldson, D. M.; Miller, N. *Trans. Faraday Soc.* **1956**, *52*, 652). It should be noted here that any primary molecular oxygen, produced directly or by track reactions, will also be measured using this method. Hence, the yields generally quoted for $HO_2^\bullet$ in the literature also include O_2. See refs 11 and 17.

(55) Watt, D. E. *Quantities for Dosimetry of Ionizing Radiations in Liquid Water*; Taylor and Francis: London, 1996. Note that, for $^{20}Ne^{9+}$ ions, we have used the stopping-power compilations of Northcliffe and Schilling (Northcliffe, L. C.; Schilling, R. F. *Nucl. Data Tables A* **1970**, *7*, 233), as suggested by LaVerne et al. (ref 19).

(56) Pimblott, S. M.; LaVerne, J. A. *J. Phys. Chem. A* **2002**, *106*, 9420.

(57) Kuppermann, A. In *Radiation Research: Proceedings of the Third International Congress of Radiation Research, Cortina d'Ampezzo, Italy, June 26-July 2, 1966*; Silini, G., Ed.; North-Holland Publishing Co.: Amsterdam, 1967; p 212.

(58) Gardès-Albert, M.; Jore, D.; Abedinzadeh, Z.; Rouscilles, A.; Deycard, S.; Bouffard, S. *J. Chim. Phys.* **1996**, *93*, 103.

(59) Olivera, G. H.; Caraby, C.; Jardin, P.; Cassimi, A.; Adoui, L.; Gervais, B. *Phys. Med. Biol.* **1998**, *43*, 2347.

(60) Taube, H. *Trans. Faraday Soc.* **1957**, *53*, 656.

(61) Biedenkapp, D.; Hartshorn, L. G.; Bair, E. J. *Chem. Phys. Lett.* **1970**, *5*, 379.

(62) Amichai, O.; Treinin, A. *Chem. Phys. Lett.* **1969**, *3*, 611.

(63) Clifford, P.; Green, N. J. B.; Oldfield, M. J.; Pilling, M. J.; Pimblott, S. M. *J. Chem. Soc., Faraday Trans. 1* **1986**, *82*, 2673. Pimblott, S. M.; Pilling, M. J.; Green, N. J. B. *Radiat. Phys. Chem.* **1991**, *37*, 377. Pimblott, S. M.; Green, N. J. B. *Res. Chem. Kinet.* **1995**, *3*, 117.

(64) Goulet, T.; Fraser, M.-J.; Frongillo, Y.; Jay-Gerin, J.-P. *Radiat. Phys. Chem.* **1998**, *51*, 85.

(65) Lundström, T.; Christensen, H.; Sehested, K. *Radiat. Phys. Chem.* **2004**, *69*, 211.

(66) Bjergbakke, E.; Draganić, Z. D.; Sehested, K.; Draganić, I. G. *Radiochim. Acta* **1989**, *48*, 65.

(67) Buxton, G. V.; Greenstock, C. L.; Helman, W. P.; Ross, A. B. *J. Phys. Chem. Ref. Data* **1988**, *17*, 513.

(68) Jiang, P.-Y.; Katsumura, Y.; Nagaishi, R.; Domae, M.; Ishikawa, K.; Ishigure, K.; Yoshida, Y. *J. Chem. Soc., Faraday Trans.* **1992**, *88*, 1653.

(69) Goldstein, S.; Czapski, G.; Cohen, H.; Meyerstein, D. *Inorg. Chim. Acta* **1992**, *192*, 87.

(70) Tang, Y.; Thorn, R. P.; Mauldin, R. L., III; Wine, P. H. *J. Photochem. Photobiol. A* **1988**, *44*, 243.

(71) Chen, R.; Avotinsh, Y.; Freeman, G. R. *Can. J. Chem.* **1994**, *72*, 1083.

(72) Neta, P.; Huie, R. E.; Ross, A. B. *J. Phys. Chem. Ref. Data* **1988**, *17*, 1027.

(73) Cabelli, D. E.; Bielski, B. H. J.; Holcman, J. *J. Am. Chem. Soc.* **1987**, *109*, 3665.

(74) Bielski, B. H. J.; Cabelli, D. E.; Arudi, R. L.; Ross, A. B. *J. Phys. Chem. Ref. Data* **1985**, *14*, 1041.

(75) Bjergbakke, E.; Sehested, K.; Rasmussen, O. L. *Radiat. Res.* **1976**, *66*, 433.

(76) Johnson, G. R. A.; Nazhat, N. B. *J. Chem. Soc., Faraday Trans. 1* **1984**, *80*, 3455.

(77) Gogolev, A. V.; Shilov, V. P.; Fedoseev, A. M.; Pikaev, A. K. *Mendeleev Commun.* **1993**, 155.

(78) See, for example: Robinson, R. A.; Stokes, R. H. *Electrolyte Solutions. The Measurement and Interpretation of Conductance, Chemical Potential and Diffusion in Solutions of Simple Electrolytes*, 2nd ed. (revised); Butterworth Publications Ltd.: London, 1959; p 229.

(79) A detailed description of our simulations of the radiolysis of aqueous solutions under acidic conditions will be given elsewhere.

(80) See, for example: Latimer, C. J. *Adv. At. Mol. Opt. Phys.* **1993**, *30*, 105.

(81) Baldacchino, G.; Bouffard, S.; Balanzat, E.; Gardès-Albert, M.; Abedinzadeh, Z.; Jore, D.; Deycard, S.; Hickel, B. *Nucl. Instrum. Methods Phys. Res. B* **1998**, *146*, 528.

(82) Wasselin-Trupin, V.; Baldacchino, G.; Bouffard, S.; Hickel, B. *Radiat. Phys. Chem.* **2002**, *65*, 53.

(83) Elliot, A. J.; Chenier, M. P.; Ouellette, D. C.; Koslowsky, V. T. *J. Phys. Chem.* **1996**, *100*, 9014.

(84) LaVerne, J. A. In *Radiation Research: Proceedings of the 11th International Congress of Radiation Research, Dublin, Ireland, July 18−23, 1999*, Vol. 2; Moriarty, M., Mothersill, C., Seymour, C., Edington, M., Ward, J. F., Fry, R. J. M., Eds.; Allen Press: Lawrence, KS, 2000; p 46.

(85) For kinetic energies of ions small compared to their rest-mass energy, the nonrelativistic Bethe stopping power equation (see: Bethe, H.

A.; Ashkin, J. In *Experimental Nuclear Physics*, Vol. 1; Segrè, E., Ed.; Wiley: New York, 1953; p 166) is well approximated by (in SI units):

$$-\frac{dE}{dx} = \left(\frac{1}{4\pi\epsilon_0}\right)^2 \frac{4\pi Z^2 e^4}{m_0 V^2} N \ln\left(\frac{2m_0 V^2}{I}\right)$$

where Ze is the charge on the incident ion, V is the ion velocity, m_0 is the rest mass of an electron, N is the number of electrons per m^3 of the absorbing medium, and I is the mean excitation and ionization potential of the bound electrons in the absorber (for liquid water, $I = 79.7 \pm 0.5$ eV, see: Bichsel, H.; Hiraoka, T. *Nucl. Instrum. Methods Phys. Res. B* **1992**, *66*, 345). It follows from this equation that for two different ions of equal LET, the one with the higher charge will have the higher velocity.

(86) Schuler, R. H.; Allen, A. O. *J. Am. Chem. Soc.* **1957**, *79*, 1565.

(87) Sauer, M. C., Jr.; Schmidt, K. H.; Hart, E. J.; Naleway, C. A.; Jonah, C. D. *Radiat. Res.* **1977**, *70*, 91.

(88) Naleway, C. A.; Sauer, M. C., Jr.; Jonah, C. D.; Schmidt, K. H. *Radiat. Res.* **1979**, *77*, 47.

(89) Kaplan, I. G.; Miterev, A. M. In *Advances in Chemical Physics*, Vol. 68; Prigogine, I., Rice, S. A., Eds.; Wiley: New York, 1987; p 255.

(90) Ferradini, C. In *Actions Biologique et Chimique des Radiations Ionisantes*, Vol. 1; Tilquin, B., Ed.; Éditions Ciaco: Bruxelles, 1990; p 52.

(91) Mozumder, A.; Magee, J. L. *Radiat. Res.* **1966**, *28*, 203; *J. Chem. Phys.* **1966**, *45*, 3332.

(92) We recall here that, like molecular oxygen, the free oxygen atom is a biradical and has two unpaired electrons.

(93) Sims, H. E.; Ashmore, C. B.; Tait, P. K.; Walters, W. S. In *Proceedings of JAIF (Japan Atomic Industrial Forum, Inc.) International Conference on Water Chemistry in Nuclear Power Plants, Kashiwazaki, Japan, October 13−16, 1998*; p 894.

(94) LaVerne, J. A.; Yoshida, H. *J. Phys. Chem.* **1993**, *97*, 10720.

(95) Bisby, R. H.; Cundall, R. B.; Sims, H. E.; Burns, W. G. *Faraday Discuss. Chem. Soc.* **1977**, *63*, 237.

(96) Baverstock, K. F.; Cundall, R. B.; Burns, W. G. In *Proceedings of the Third Tihany Symposium on Radiation Chemistry, Balatonfüred-Tihany, Hungary, May 10−15, 1971*, Vol. 2; Dobó, J., Hedvig, P., Eds.; Akadémiai Kiadó: Budapest, 1972; p 1133.

(97) Boyle, J. W.; Hochanadel, C. J.; Sworski, T. J.; Ghormley, J. A.; Kieffer, W. F. In *Proceedings of the International Conference on the Peaceful Uses of Atomic Energy, Geneva, Switzerland, August 1955*, Vol. 7, P/741; United Nations: New York, 1956; p 576.

(98) Steele, L. R.; Gordon, S.; Dryden, C. K. *Nucl. Sci. Eng.* **1963**, *15*, 458.

(99) Meesungnoen, J.; Jay-Gerin, J.-P.; Filali-Mouhim, A.; Mankhetkorn, S. *Chem. Phys. Lett.* **2001**, *335*, 458.

(100) See, for example: Hall, E. J. *Radiobiology for the Radiologist*, 5th ed.; Lippincott Williams & Wilkins: Philadelphia, 2000; p 91.

(101) We can cite here the elegant work of Barendsen et al. (Barendsen, G. W.; Koot, C. J.; van Kersen, G. R.; Bewley, D. K.; Field, S. B.; Parnell, C. J. *Int. J. Radiat. Biol.* **1966**, *10*, 317), who used cultured cells of human origin to investigate the OER for a wide range of radiation types. These authors showed that as the LET increases, the OER falls slowly at first, from ~2.6 to 2.05 between ~5.6 and 61 keV/μm, after which the OER decreases more rapidly and approaches unity at an LET value of ~165 keV/μm.

(102) Alper, T.; Bryant, P. E. *Int. J. Radiat. Biol.* **1974**, *26*, 203. Bryant, P. E.; Alper, T. In *Proceedings of the 5th Symposium on Microdosimetry, Verbania Pallanza, Italy, September 22−26, 1975*, Report EUR 5452 (for de−en−fr); Booz, J., Ebert, H. G., Smith, B. G. R., Eds.; Commission of the European Communities: Luxembourg, 1976; p 871.

(103) Neary, G. J. *Int. J. Radiat. Biol.* **1965**, *9*, 477. See also: Swallow, A. J.; Velandia, J. A. *Nature* **1962**, *195*, 798.

(104) Baverstock, K. F.; Burns, W. G. *Radiat. Res.* **1981**, *86*, 20.

(105) Stuglik, Z. *Radiat. Res.* **1995**, *143*, 1995. See also, for example: Michael, B. D.; Prise, K. M. *Int. J. Radiat. Biol.* **1996**, *69*, 351. Frankenberg-Schwager, M.; Frankenberg, D.; Harbich, R.; Beckonert, S. *Radiat. Environ. Biophys.* **1994**, *33*, 1. Kiefer, J. *Biological Radiation Effects*; Springer-Verlag: Berlin, 1990; p 157. Jonah, C. D. *Radiat. Res.* **1985**, *104*, S-47. Sauer, M. C., Jr.; Schmidt, K. H.; Jonah, C. D.; Naleway, C. A.; Hart, E. J. *Radiat. Res.* **1978**, *75*, 519.

(106) Lefort, M. In *Actions Chimiques et Biologiques des Radiations*, Vol. 1; Haïssinsky, M., Ed.; Masson: Paris, 1955; p 93, and references therein.

(107) Allen, A. O. *Radiat. Res. Suppl.* **1964**, *4*, 54.

(108) Burns, W. G.; May, R.; Baverstock, K. F. *Radiat. Res.* **1981**, *86*, 1.

(109) LaVerne, J. A.; Schuler, R. H. *J. Phys. Chem.* **1996**, *100*, 16034.

(110) Senvar, C. B.; Hart, E. J. In *Proceedings of the Second United Nations International Conference on the Peaceful Uses of Atomic Energy, Geneva, Switzerland, September 1−13, 1958*, Vol. 29, P/1128; United Nations: Geneva, 1958; p 19.

(111) Examination of the material balance equation between the "reducing" (e^-_{aq}, $H^\bullet$, and H_2) and "oxidizing" ($^\bullet OH$, H_2O_2, $HO_2^\bullet/O_2^{\bullet-}$, O_2, etc.) species formed in the decomposition of pure, deaerated liquid water can also serve as a criterion for a consistent set of G-values. Under high-LET, heavy-ion irradiation conditions, this equation (refs 11 and 30):

$$G_{e^-_{aq}} + G_{H^\bullet} + 2\,G_{H_2} = G_{^\bullet OH} + 2\,G_{H_2O_2} + 3\,G_{HO_2^\bullet/O_2^{\bullet-}} + 4\,G_{O_2} + \ldots$$

is found to be well satisfied by the results of our simulations throughout the range of LET values studied here.

(112) Interestingly, Brown et al. (Brown, W. G.; Hart, E. J.; Sauer, M. C., Jr. *Radiat. Res.* **1978**, *76*, 533) measured the production of the $O(^3P)$ atom in the radiolysis of water by 20 MeV $^2H^+$ (LET ~ 10 keV/μm) and 40 MeV $^4He^{2+}$ (LET ~ 37 keV/μm) ions, using the reaction of $O(^3P)$ with cyclopentene. The values that these authors obtained for $G[O(^3P)]$ are ~0.0047 and 0.0045 molec./100 eV for deuterons and helium ions, respectively. They also estimated the characteristic time of their measurements (inverse of the cyclopentene scavenging power) to be $\sim 5 \times 10^{-8}$ s. These experimental data can directly be compared with the results of our simulations. In fact, when the multiple ionization of water is included in the calculations, we find that, at 5×10^{-8} s, $G[O(^3P)] \approx 0.0094$ and 0.0048 molec./100 eV for ~10 keV/μm $^2H^+$ and ~37 keV/μm $^4He^{2+}$ ions, respectively. Judging from the reported experimental errors (measured yields may be on the order of 15% too low), these results are in remarkable agreement with Brown et al.'s experiments.

(113) We have found by independent simulations incorporating the sole mechanism of double ionization of water molecules that triply and quadruply charged water ions make in fact a negligible contribution to G_{O_2} under the conditions $\sigma_{ti} = \alpha^2\,\sigma_{si}$ and $\sigma_{qi} = \alpha^3\,\sigma_{si}$ (where $\sigma_{di}/\sigma_{si} = \alpha < 0.5$) adopted in this study (data not shown).

(114) See, for example: Zander, R. In *Proceedings of the Second International Symposium on Oxygen Transport to Tissue, Mainz, Germany, March 12−14, 1975*; Grote, J., Reneau, D. D., Thews, G., Eds.; Plenum Press: New York, 1976; p 463. Halliwell, B.; Gutteridge, J. M. C. *Free Radicals in Biology and Medicine*, 3rd ed.; Oxford University Press: Oxford, 1999; p 1. von Sonntag, C. *Free-Radical-Induced DNA Damage and its Repair − A Chemical Perspective*; Springer-Verlag: Heidelberg, 2006 (in press).